Applied Mathematical Modelling 112 (2022) 800–821

Contents lists available at ScienceDirect

Applied Mathematical Modelling

journal homepage: www.elsevier.com/locate/apm

Zonal modeling of air distribution impact on the long-range airborne transmission risk of SARS-CoV-2

Amar Aganovic[a,*], Guangyu Cao[b], Jarek Kurnitski[c], Arsen Melikov[d], Pawel Wargocki[d]

[a] Department of Automation and Process Engineering, UiT The Arctic University of Norway, Postboks 6050 Langnes, Tromsø 9037, Norway
[b] Department of Energy and Process Engineering, Norwegian University of Science and Technology - NTNU, Trondheim, Norway
[c] REHVA Technology and Research Committee, Tallinn University of Technology, Tallinn, Estonia
[d] Department of Civil Engineering, Technical University of Denmark, Copenhagen, Denmark

ARTICLE INFO

Article history:
Received 12 March 2022
Revised 15 August 2022
Accepted 25 August 2022
Available online 28 August 2022

Keywords:
Air distribution method
Wells-Riley model
Zonal modeling
Infection risk
Virus airborne transmission
SARS-CoV-2

ABSTRACT

A widely used analytical model to quantitatively assess airborne infection risk is the Wells-Riley model which is limited to complete air mixing in a single zone. However, this assumption tends not to be feasible (or reality) for many situations. This study aimed to extend the Wells-Riley model so that the infection risk can be calculated in spaces where complete mixing is not present. Some more advanced ventilation concepts create either two horizontally divided air zones in spaces as displacement ventilation or the space may be divided into two vertical zones by downward plane jet as in protective-zone ventilation systems. This is done by evaluating the time-dependent distribution of infectious quanta in each zone and by solving the coupled system of differential equations based on the zonal quanta concentrations. This model introduces a novel approach by estimating the interzonal mixing factor based on previous experimental data for three types of ventilation systems: incomplete mixing ventilation, displacement ventilation, and protective zone ventilation. The modeling approach is applied to a room with one infected and one susceptible person present. The results show that using the Wells-Riley model based on the assumption of completely air mixing may considerably overestimate or underestimate the long-range airborne infection risk in rooms where air distribution is different than complete mixing, such as displacement ventilation, protected zone ventilation, warm air supplied from the ceiling, etc. Therefore, in spaces with non-uniform air distribution, a zonal modeling approach should be preferred in analytical models compared to the conventional single-zone Wells-Riley models when assessing long-range airborne transmission risk of infectious respiratory diseases.

1. Introduction

Severe Acute Respiratory Syndrome Coronavirus 2 (SARS-CoV-2) and the disease it causes (COVID-19) pose a threat to health security worldwide and has caused more than a million deaths (Feb. 2022) since the beginning of the pandemic

* Corresponding author.
E-mail address: amar.aganovic@uit.no (A. Aganovic).

https://doi.org/10.1016/j.apm.2022.08.027

Nomenclature

A_{per}	surface area of average adult (m^2)
β	dimensionless measure of the degree of mixing (mixing factor) between zones i and j in both directions (–)
C_{ds}	drag coefficient at sedimentation (-)
c_v	viral load in the sputum ($\frac{RNA}{ml}$)
c_v	viral load in the sputum ($\frac{RNA}{ml}$)
D	deposition by gravitational settling ($\frac{1}{h}$)
DE	total deposition number (%)
D_{eq}	the droplet equilibrium diameter (m)
ε	ventilation efficiency (–)
g	gravitational acceleration ($\frac{m}{s^2}$)
γ	dimensionless measure of the degree of mixing (mixing factor) between zones j and k in both directions (–)
H	room height (m)
h_{per}	height of average adult (m)
I	number of infected persons (–)
IR	inhalation rate ($\frac{m^3}{h}$)
k	inactivation by biological decay ($\frac{1}{h}$)
$n\,(t)$	quanta concentration in the indoor environment at the time (t) ($\frac{quanta}{m^3}$)
$n_{exh}\,(t)$	quanta concentration in the in the exhaust at the time (t) ($\frac{quanta}{m^3}$)
$n_i\,(t)$	quanta concentration in zone i at the time (t) ($\frac{quanta}{m^3}$)
$n_j(t)$	quanta concentration in zone j at the time (t) ($\frac{quanta}{m^3}$)
$n_k(t)$	quanta concentration in zone k at the time (t) ($\frac{quanta}{m^3}$)
N_i	droplet number concentration in the ith bin ($\frac{particles}{cm^3}$)
$n_{sup}\,(t)$	quanta concentration in the in the supply/outdoor at the time (t) ($\frac{quanta}{m^3}$)
ζ	respiratory absorption ($\frac{1}{h}$)
P	infection risk (%)
P_{per}	heat output from average adult (m^2)
Q_{conv}	convective airflow rate from heat load in room ($\frac{m^3}{h}$)
$Q_{i\,-\,j}$	airflow movement from zone i to zone j ($\frac{m^3}{h}$)
$Q_{j\,-\,i}$	airflow movement from zone j to zone i ($\frac{m^3}{h}$)
$Q_{j\,-\,k}$	airflow movement from zone j to zone k ($\frac{m^3}{h}$)
$Q_{sup} = Q_{exh}$	supply/exhaust airflow rate to/from the room ($\frac{m^3}{h}$)
R	resuspension ($\frac{1}{h}$)
ρ_d	density of droplets ($\frac{kg}{m^3}$)
ρ_a	density of air ($\frac{kg}{m^3}$)
S	source term ($\frac{quanta}{h}$)
ΔT	temperature difference between supply and exhaust air (K)
Φ	factor determining the number of quanta emitted in the lower i zone (–)
V	room volume (m^3)
V_i	the mean volume of a single droplet in the ith bin (mL)
y_n	height of neutral zone (m)

in 2020 [1]. SARS-CoV-2 can infect a person through exposure to respiratory fluids carrying the infectious virus. This can happen either by being exposed to infectious droplets and particles (aerosols) in the surrounding air or touching surfaces contaminated by infectious respiratory fluid [2]. The evidence for the airborne transmission of SARS-CoV-2 contained in aerosols has grown as the pandemic progressed [3–7]. It is now widely accepted that airborne transmission of SARS-CoV-2 may be the leading cause of super spreading events that are recognized as the pandemic's primary drivers [8–10]. The preventive measures in indoor environments should include decreasing the risks because of airborne transmission, among others obtained by ventilation. To this end, validated and well-performing predictive mathematical models and risk assessment create fundamental tools for understanding and planning effective strategies to minimize risks associated with airborne transmission.

Wells-Riley is the classical and widely used model to quantitatively assess airborne infection risk (Wells [11] and Riley et al. [12]). The Wells-Riley model presents a quick and straightforward evaluation method that implicitly calculates the airborne infection risk using the concept of quantum - one quantum is defined as the number of inhaled infectious droplet nuclei or the infectious dose required to infect 63.2% of susceptible persons in an enclosed space. The Wells-Riley model has extensively been used to evaluate the airborne infection risk of respiratory diseases, such as tuberculosis [13], measles [14], influenza [15], H1N1 [16], and more recently, SARS-CoV-2 [17,18]. However, the original Wells-Riley model is based on the well-mixed room air and steady-state generation of airborne pathogens, which may not be the case in real environments. Consequently, the airborne infection risk could be under-or overestimated [19,20]. Non-steady state solutions for the Wells-Riley model have been developed in the form of differential equations by Gammaitoni and Nucci [21] and alternative equations in a study by Rudnick and Milton [22] that introduced the concept of exhaled air volume fraction, which requires measuring CO_2 concentrations. These non-steady-state solutions still adopt the well-mixed assumption that is not the principle of advanced and novel ventilation systems such as displacement ventilation as they do not create a uniform indoor air distribution [23,24]. In buildings with such systems, the risk of airborne transmission examined by the conventional Wells-Riley model can be led to flawed interpretations [25].

Various modifications have been proposed to overcome the well-mixing limitation to account for the spatial distribution of infection risk when using the Wells-Riley model [26–30]. One of the first solutions to this problem was presented by Ko et al. [26]. They used a theoretical model expansion of the Wells-Riley model, in which the enclosed space of an airliner was divided into multiple cabins (or zones). In this way, the degree of exposure to airborne infectious pathogens could be varied from cabin to cabin and better estimated. While this zone-model approach seems operational and reasonably simple, it does not consider the type of airflow distribution. Therefore, it is not easy to extrapolate this concept to other applications than the original use in the aircraft cabin. The Wells-Riley multi-zonal approach has been extensively applied to hospital environments in several studies by Noakes et al. [27–30]. While these studies consider the role of interzonal airflow distribution on the risk of airborne infection in multizonal departments such as adjacent hospital wards and corridors, the proposed models share the following limitations i) steady-state computation of quanta concentration in each zone is applied to the Wells-Riley models ii) the assumption of the interzonal-mixing factor value was selected based on CFD simulations for specific case-scenarios. In addition, modeling advanced airflow distribution methods such as displacement or protected zone ventilation was not within the scope of these studies.

Recent studies that consider the spatial distribution of infection risk calculated by the Wells-Riley model use numerical simulations (CFD) [31–37] or tracer gas measurements [38]. However, the CFD approach requires comprehensive information on the room configuration and ventilation design conditions and has limitations on a time-consuming simulation process. The tracer-gas measurements, on the other hand, require both an experimental setup and measurement equipment and have lower predictive capacity.

Therefore, the objective of the present study is to extend the Wells-Riley model so that it can be used for quick and straightforward infection-risk calculations in spaces where complete air mixing is not present. The models presented in this study are based on the zonal modeling approach presented in works by Noakes et al. [27–30]. However, the novelty of the multi-zonal approach presented in this study compared to the previous works [27–30] include: (i) transient-state computation of quanta concentration is presented for each zone (ii) the interzonal mixing factor is calculated based on the ventilation efficiency values derived from literature (iii) solutions for advanced airflow distribution methods such as displacement ventilation and protective zone ventilation are presented.

2. Methodology

2.1. Approach

The model presented in this study is loosely based on the zonal models developed by Nicas [39] and Sandberg [40], in which the enclosed spaces are divided into zones with uniformed mixed air. In this study, the zonal modeling approach is used to demonstrate the impact of different airflow distribution methods on the infection risk in an enclosed space occupied by one infected and one susceptible person. The development of this model is carried out in the following manner (Fig. 1): the enclosed space is first divided into vertical or horizontal zones depending on the position of airflow supply and exhaust according to the considered airflow distribution methods. The next step is to express the interzonal airflow mixing factor between the two zones β as a function of the ventilation efficiency ε. This allows solving the set of differential equations representing the time-dependent distribution of infectious quanta in each zone by using the interzonal mixing factor β expressed as a function of the ventilation efficiency ε. Finally, based on the calculated zonal quanta concentrations from the previous step, the zonal infection risk may be calculated according to the Wells-Riley equation.

2.2. The Wells-Riley model extension assumptions

For this study, we assumed two-zone airflow distribution methods with horizontal and vertical zoning in the enclosed space and the airflow distribution methods classified as incomplete mixing ventilation, displacement ventilation, and protected zone ventilation (Fig. 2).

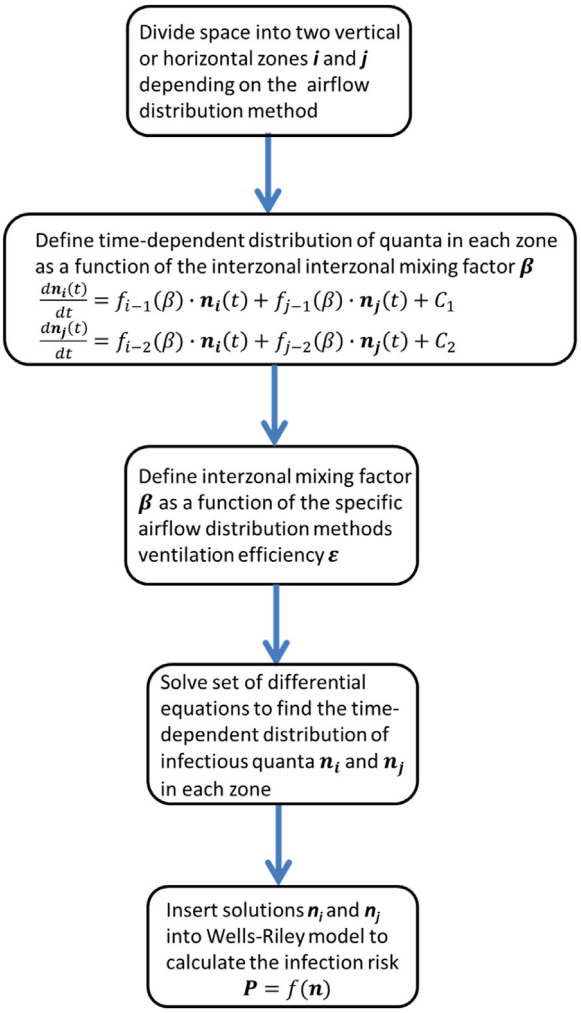

Fig. 1. Methodology approach.

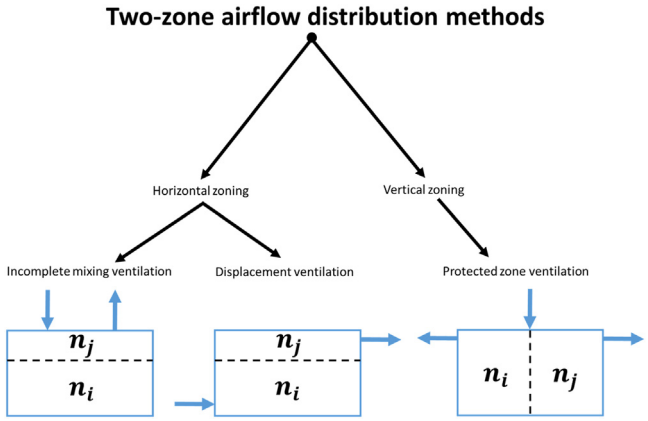

Fig. 2. A schematic presentation of the airflow distribution methods considered in the extended version of the Wells-Riley model in an enclosed space; ni and nj show time-dependent quanta concentrations in each zone.

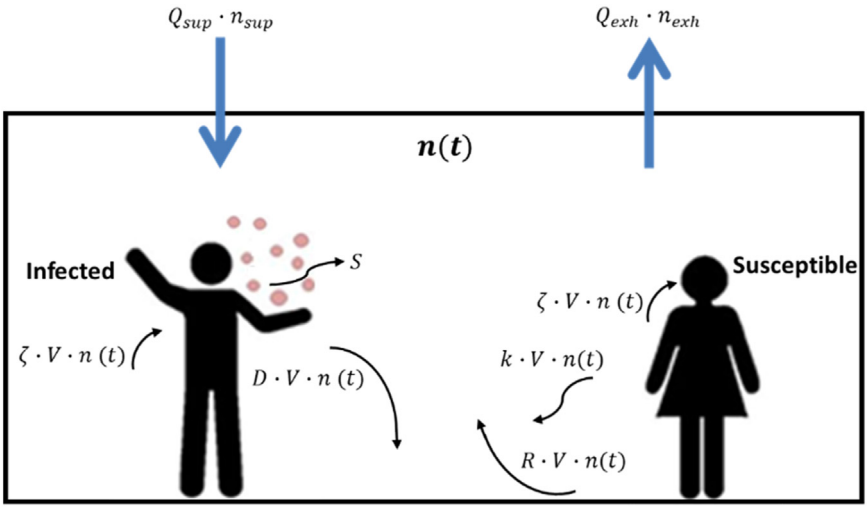

Fig. 3. Schematic representation of a simple indoor air mass-balance model in case of a completely mixed room.

For each of the airflow distribution methods represented by the different ventilation systems, the following assumptions were made:

(i) The only emission source of SARS-CoV-2 is from the infected individual within the room who emits SARS-CoV-2 quanta at a constant rate.
(ii) There are four removal mechanisms of the infectious quanta: deposition by gravitational settling, virus inactivation by biological decay, respiratory absorption, and ventilation with recirculation; resuspension rate R is neglected in the model($R \approx 0$).
(iii) Indoor airborne transmission is associated with aerosol droplets $\leq 5\ \mu$m in the dehydrated state [41].
(iv) Only long-range (>1.5 m) airborne transmission is considered [42]
(v) The volumetric flow rates of air into the room from outside and out of the room to the outside are assumed to be equal and constant for the duration of the analysis, so the systems are considered balanced concerning the inward and outward flows.
(vi) Infectious respiratory airborne droplets become evenly distributed throughout each zone considered after reaching steady-state conditions, so for each zone complete mixing is assumed.
(vii) No virus-laden airborne particles enter the supplied air (from the outside) ($n_{sup} = 0$).
(viii) There is no prior source of infectious aerosol in space.
(ix) The viral content of a saliva droplet produced by an infected person is proportional to its initial volume [43].
(x) There is no simulated sunlight indoors (ultraviolet B solar irradiance $\approx$ 0 W/m^2).

2.3. Mixing ventilation

A schematic representation of the theoretical model assessing the impact of the airflow distribution method on the quanta emission rate of SARS-CoV-2 for infection risk assessment in case of the mixing ventilation is shown in Fig. 3.

The differential Eq. (1) represents the mass balance single-zone model for a completely mixed mechanically ventilated room:

$$V \cdot \frac{dn(t)}{dt} = S + Q_{sup} \cdot n_{sup}(t) - Q_{exh} \cdot n_{exh}(t) - k \cdot n(t) \cdot V - D \cdot V \cdot n(t) - R \cdot V \cdot n(t) - 2 \cdot \zeta \cdot V \cdot n(t) \quad (1)$$

Since tracer gas has been confirmed as a suitable surrogate for the exhaled droplet nuclei $<5\ \mu m$ when studying the airborne transmission in the built environment [44,45], we will use the Eq. (2) [42] to express the ventilation efficiency for removing droplet nuclei represented by a tracer gas concentration C from an indoor space under steady-state conditions, i.e. from the moment the quanta concentration in the occupied zone $n(t)$ has reached the steady-state level:

$$\varepsilon = \frac{C_{exh} - C_{sup}}{C - C_{sup}} = \frac{n_{exh}(t) - n_{sup}(t)}{n(t) - n_{sup}(t)} \quad (2)$$

For a completely mixed condition, the ventilation efficiency is $\varepsilon = 1$. Under this condition, the quanta level in the exhaust equals the quanta level in the room ($n_{exh}(t) = n(t)$) and by assuming that viruses in the supplied air are absent ($n_{sup} = 0$ the differential Eq. (1) can be reduced to

$$V \cdot \frac{dn(t)}{dt} = S - Q \cdot n(t) - V \cdot k \cdot n(t) - V \cdot D \cdot n(t) - 2 \cdot V \cdot \zeta \cdot n(t) \quad (3)$$

To solve Eq. (4) in the form of a first-order differential equation $\frac{dn(t)}{dt} + n(t) \cdot a = b$, the equation may be rewritten as follows:

$$\frac{dn(t)}{dt} + n(t) \cdot \left(\frac{Q}{V} + D + k + 2 \cdot \zeta \right) = \frac{S}{V} \tag{4}$$

The unique solution of quanta concentration *n(t)* in an indoor environment with complete mixing ventilation at time t is:

$$n(t) = n_0 \cdot e^{-\left(\frac{Q}{V}+D+k+2\cdot\zeta\right)\cdot t} + \frac{S}{V} \cdot \left\{ \frac{1}{\frac{Q}{V}+D+k+2\cdot\zeta} - \frac{1}{\frac{Q}{V}+D+k+2\cdot\zeta} \cdot e^{-\left(\frac{Q}{V}+D+k+2\cdot\zeta\right)\cdot t} \right\} \tag{5}$$

where n_0 is the initial quanta concentration ($\frac{quanta}{m^3}$) at time t = 0.

To perform calculations with Eq. (5) and to predict indoor concentrations of quanta at time *t*, appropriate expressions for the source term *S*, deposition rate *D*, inactivation rate *k*, and absorption rate ζ and must be first be known.

To determine the probability of infection (*P*, %) as a function of the exposure time (*t*) of susceptible people, the quanta concentration must be integrated over time through the Wells–Riley equation as follows:

$$P = \left(1 - e^{-IR \int_0^T n(t)dt} \right) (\%) \tag{6}$$

2.4. Incomplete mixing ventilation

The contaminant distribution modeling approach in indoor spaces with incomplete mixing is based on two-zone models, in which the space under consideration is divided horizontally into two perfectly mixed zones, Fig. 3. This phenomenon occurs due supplying heated air from a ceiling-mounted supply inlet [40,46]. Besides the inter-zonal mixing factor, the main unknown variable that needs to be determined in this modeling approach is the volume of the two zones. Previous studies have shown relatively uniform concentrations and airflow distributions established in the volume that may be identified as the occupied zone, i.e. up to around 1.8 m height from the floor [40,46,47]. But no general means of identifying the exact volumes of the two zones have been proposed. Therefore, the model for incomplete mixing ventilation in this study is also based on the assumption that the volume of an incompletely mixed room will be divided into the lower or occupied zone having a height of H = 1.8 m and the upper zone which consists of the rest of the room volume.

Fig. 4 shows a schematic presentation of a two-zone exposure model for the room with an incomplete mixing loosely based on the two-zone models for the incomplete mixing used earlier in the literature [30,36]. In the exposure model, the space under consideration is divided horizontally into two perfectly mixed zones with uniform quanta concentrations in each zone $n_i(t)$ and $n_j(t)$: the occupied zone *i* reaching $h_{occup.} = 1.8\,m$ above the floor and the rest is the unoccupied zone $n_j(t)$. The volume of the occupied zone can be expressed as $V_i = \frac{1.8}{H} \cdot V$, where H is the height of the space, while the volume of the unoccupied zone is $V_j = (1 - \frac{1.8}{H}) \cdot V$ .The airflow mixing between the two zones is presented by the inter-zonal airflow rates Q_{i_j} and Q_{j_i}, where *i*-*j* denotes the zone *i*-to-zone *j* movement and *j*-*i* denotes the reverse air movement. By the principle of continuity of airflow in each zone, the inter-zonal airflow rates for this scenario must be equal, i.e. $Q_{j\_i} = Q_{i\_j} = \beta \cdot Q$ where β is a dimensionless measure of the degree of mixing (mixing factor) between zones *i* and *j* in both directions.

The quanta balance for the lower occupied zone *i* can be expressed in the following form:

$$V_i \cdot \frac{dn_i(t)}{dt} = S + \beta \cdot Q \cdot n_j(t) - \beta \cdot Q \cdot n_i(t) - k \cdot n_i(t) \cdot V_i - D \cdot V_i \cdot n_i(t) - 2 \cdot \zeta \cdot V_i \cdot n_i(t) \tag{7}$$

and after regrouping:

$$\frac{dn_i(t)}{dt} = \left(-\frac{\beta \cdot Q \cdot H}{1.8 \cdot V} - k - D - 2 \cdot \zeta \right) \cdot n_i(t) + \frac{\beta \cdot Q \cdot H}{1.8 \cdot V} \cdot n_j(t) + \frac{S \cdot H}{1.8 \cdot V} \tag{8}$$

The quanta flow rate balance for the upper zone *j:*

$$V_j \cdot \frac{dn_j(t)}{dt} = Q \cdot n_{j,sup} - Q \cdot n_{j,exh}(t) + \beta \cdot Q \cdot n_i(t) - \beta \cdot Q \cdot n_j(t) - k \cdot n_j(t) \cdot V_j - D \cdot V_j \cdot n_j(t) \tag{9}$$

And after regrouping Eq. (9):

$$\frac{dn_j(t)}{dt} = \frac{\beta \cdot Q \cdot H}{V \cdot (H - 1.8)} \cdot n_i(t) + \left(-\frac{(\beta + 1) \cdot Q \cdot H}{V \cdot (H - 1.8)} - k - D \right) \cdot n_j(t) + \frac{Q \cdot n_{sup} \cdot H}{V \cdot (H - 1.8)} \tag{10}$$

The novelty in the zone exposure model is that the value of the mixing factor β is calculated as a function of the steady-state ventilation effectiveness, i.e. when $\frac{dn_i(t)}{dt} = \frac{dn_j(t)}{dt} = 0$. As the outdoor air is contaminant free $n_{sup} \approx 0$ and no recirculation can be considered the ventilation efficiency can be expressed as $\varepsilon = \frac{n_{exh}(t) - n_{sup}(t)}{n(t) - n_{sup}(t)} = \frac{n_j}{n_i}$. By dividing both sides

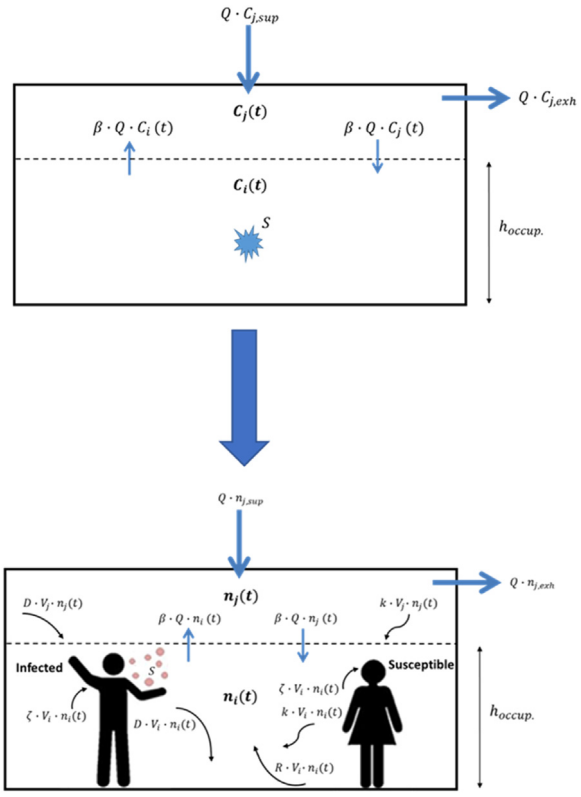

Fig. 4. Schematic representation of transforming the simplified two-zone model concept of contaminant distribution in a room with incomplete mixing ventilation [40,46] to a two-zone exposure model for assessing the long-range airborne transmission risk in indoor environments.

of Eq. (10) with n_i it becomes possible to derive an expression for the mixing factor β as a function of the ventilation effectiveness ε in the following manner:

$$\frac{\beta \cdot Q \cdot H}{V \cdot (H-1.8)} + \left(-\frac{(\beta+1) \cdot Q \cdot H}{V \cdot (H-1.8)} - k - D \right) \cdot \varepsilon = 0 => \beta = \frac{\varepsilon}{1-\varepsilon} \cdot \frac{Q \cdot H + (k+D) \cdot (H-1.8) \cdot V}{Q \cdot H} \tag{11}$$

We used measurements (n = 25) from four studies in mixing ventilated rooms with supply located in the ceiling and exhaust in the sidewall [40,46–48] to determine a linear regression model expressing the relationship between the ventilation efficiency ε and the supply airflow, the room height and the and the difference between the supply and exhaust temperatures expressed as $H^4 \cdot (\frac{\Delta T^4}{Q})^{0.1}$. This correlation is based on

$$\varepsilon = -0.0354 \cdot H^2 \cdot \left(\frac{\Delta T^4}{Q} \right)^{0.1} + 0.9542 \tag{12}$$

A fairly good fit ($R^2 = 0.76$ was obtained (Fig. 5).

2.5. Displacement ventilation

In a space with displacement ventilation, cool air is supplied at floor level so warm contaminated air is rising due to buoyancy forces and extracted at ceiling level. Theoretically, due to the thermal stratification, two zones will be formed in an indoor space: a lower, cooler, and cleaner zone and an upper warmer and contaminated zone [49]. The stratification point is located at the point where the airflow rate to the lower zone equals the airflow out from the lower zone [50]. As the heat load inside the room also creates rising convective flow, the stratification height y_n (m) will depend on the amount of airflow supplied and the convective flow from the thermal load inside the considered space and can be determined from the airflow balance for zone i:

$$Q_{sup} + \beta \cdot Q = \sum_{h=y_n} Q_{conv} + \beta \cdot Q \;\; => \;\; Q_{sup} = \sum_{h=y_n} Q_{conv} \tag{13}$$

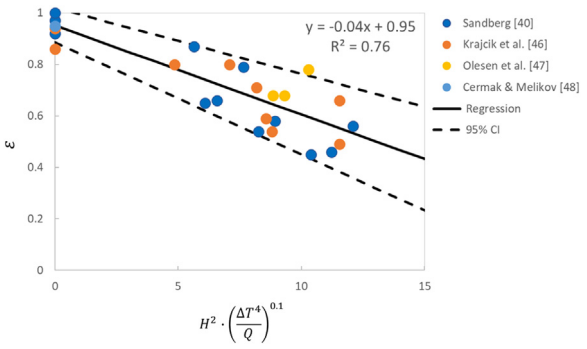

Fig. 5. A linear regression fit model for expressing the contaminant removal effectiveness ε in case of the incomplete mixing ventilation.

The convective airflow rising from I number of human adults at height $h = y_n$ can be calculated according to the following model derived by Dokka [51]:

$$\sum_{h=y_n} Q_{conv} = I \cdot 17.22 \cdot \left(-h_{per} + \sqrt{h_{per}^2 + \frac{A_{per}}{\pi}}\right) \cdot \left(\frac{P_{per}}{A_{per}}\right)^{0.3} \cdot y_n^{1.2} \tag{14}$$

The surface area of an average adult A_{per} can be set at 1.8 m^2 [52]. The height of an average adult h_{per} seated and standing can be respectively set at 1.2 m and 1.75 m. At normal room temperature conditions with normal indoor clothing and activity the convective part of the sensible heat output P_{per} of a person can be estimated at 50 % [54].

The neutral height y_n has to be iterated in Eq. (13) until the sum of the convective airflows from the thermal load equals the supply airflow rate, i.e., $\sum_{h=y_n} Q_{conv} = Q_{sup}$. As the stratification height across the inter-zonal cross-section will vary, we will define a share factor Φ that defines the amount of the quanta that is emitted in the lower zone $\Phi \cdot S$ and the amount of the quanta emitted from the infected person in the upper zone $(1 - \Phi) \cdot S$. When $y_{st} >$ breathing/exhalation zone of the infected person then $\Phi = 0$, and vice versa: when $y_n <$ breathing/exhalation zone of the infected manikin then $\Phi = 1$.

The quanta flow rate balance for the lower zone *i:*

$$V_i \cdot \frac{dn_i(t)}{dt} = (1 - \Phi) \cdot S + Q_{sup} \cdot n_{i,sup} - (\beta + 1) \cdot Q \cdot n_i(t) + \beta \cdot Q \cdot n_j(t) - k \cdot n_i(t) \cdot V_i - D \cdot V_i \cdot n_i(t) - 2 \cdot \zeta \cdot V_i \cdot n_i(t) \tag{15}$$

$$\frac{dn_i(t)}{dt} = \left(-\frac{(\beta + 1) \cdot Q \cdot H}{y_n \cdot V} - k - D - 2 \cdot \zeta\right) \cdot n_i(t) + \frac{\beta \cdot Q \cdot H}{y_n \cdot V} \cdot n_j(t) + \frac{(1 - \Phi) \cdot S \cdot H}{y_n \cdot V} + \frac{Q \cdot n_{sup} \cdot H}{y_n \cdot V} \tag{16}$$

The quanta flow rate balance for the upper zone *j:*

$$V_j \cdot \frac{dn_j(t)}{dt} = \Phi \cdot S + (\beta + 1) \cdot Q \cdot n_i(t) - (\beta + 1) \cdot Q \cdot n_j(t) - k \cdot n_j(t) \cdot V_j - D \cdot V_j \cdot n_j(t) - 2 \cdot \zeta \cdot V_j \cdot n_j(t) \tag{17}$$

or when expressed in the form of a first-order differential equation:

$$\frac{dn_j(t)}{dt} = \frac{(\beta + 1) \cdot Q \cdot H}{V \cdot (H - y_n)} \cdot n_i(t) + \left(-\frac{(\beta + 1) \cdot Q \cdot H}{V \cdot (H - y_n)} - k - D - 2 \cdot \zeta\right) \cdot n_j(t) + \frac{\Phi \cdot S \cdot H}{V \cdot (H - y_n)} \tag{18}$$

Similarly, as for incomplete mixing ventilation, an expression for the displacement ventilation mixing factor as a function of the contaminant removal effectiveness ε was derived ($n_{sup} \approx 0$):

If $y_n < y_{infected\_exhalation} \Rightarrow \Phi = 1$ then

$$\beta = \frac{1}{\varepsilon - 1} \cdot \frac{Q \cdot H + (k + D + 2 \cdot \zeta) \cdot y_n \cdot V}{Q \cdot H} \tag{19}$$

We used data (n = 30) from seven studies [53–59] to create a polynomial linear regression model expressing the relationship between the reported normalized concentrations $\frac{C_i}{C_j}$ (which is equal to the inverse value of contaminant removal effectiveness ε^{-1}) and the parameter $\left(\frac{\Delta T \cdot Q}{V}\right)^{0.4}$ based on

$$\varepsilon = \frac{1}{-0.32 \cdot \left(\frac{\Delta T \cdot Q}{V}\right)^{0.33} + 1.00} \tag{20}$$

A fairly strong fit ($R^2 = 0.71$) was obtained (Fig. 7)

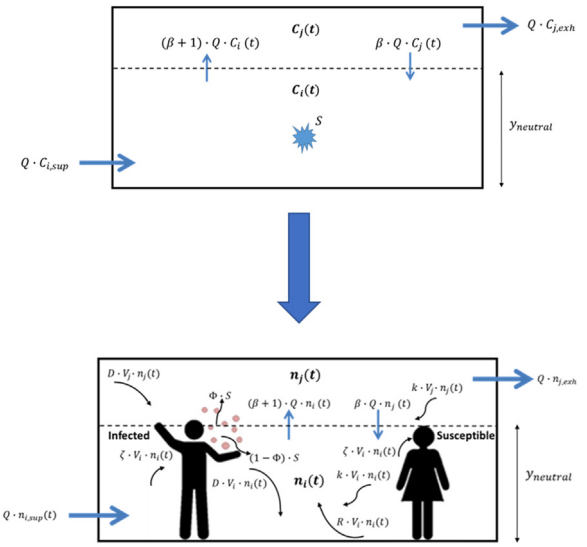

Fig. 6. Schematic representation of transforming the simplified two-zone model concept of contaminant distribution for displacement ventilation [40] to a two-zone exposure model for assessing the long-range airborne transmission risks in indoor environments.

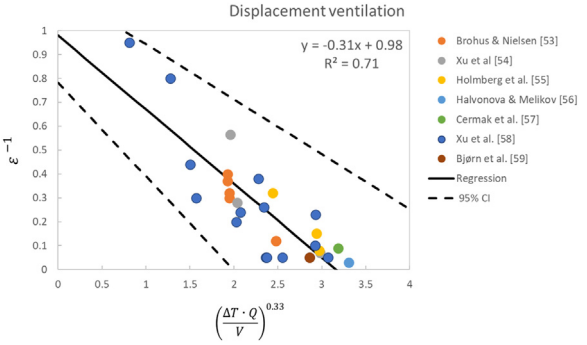

Fig. 7. A linear regression fit model for expressing the inverse value of the ventilation efficiency ε for displacement ventilation.

2.6. Protected zone ventilation

The protected zone ventilation [60] separates an indoor space into two well-mixed subzones i and j of equal volume ($V_i = V_j = \frac{V}{2}$) by using a downward plane jet as shown in Fig. 6. We will assume that due to the uniformity of the airflow distribution from the jet plane, each zone will be supplied by an equal amount of the total airflow supply rate, i.e. $Q_{i,sup} = Q_{j,sup} = \frac{Q_{sup}}{2} = \frac{Q}{2}$ and that an equal amount of air will be extracted from each zone $Q_{i,exh} = Q_{j,exh} = \frac{Q_{sup}}{2} = \frac{Q}{2}$. As a consequence, the inter-zonal airflow rates will be equal, i.e. $Q_{i\_j} = Q_{j\_i} = \beta \cdot Q$, where β is the mixing factor between zones i and j. A simplified two-zone model concept of contaminant distribution for protected zone ventilation transformed into a two-zone exposure model for assessing the long-range airborne transmission risks in indoor environments is shown in Fig. 8.

The quanta flow rate balance for the polluted zone *i:*

$$V_i \cdot \frac{dn_i(t)}{dt} = S + Q_{i,sup}\cdot n_{sup}(t) + \beta\cdot Q\cdot n_j(t) - Q_{i,exh}\cdot n_{i,exh}(t) - \beta\cdot Q\cdot n_i(t) - k\cdot n_i(t)\cdot V_i - D\cdot V_i\cdot n_i(t) - \zeta\cdot V_i\cdot n_i(t) \quad (21)$$

and after regrouping becomes using expression (21) becomes:

$$\frac{dn_i(t)}{dt} = \left(-\frac{2\cdot\beta\cdot Q + Q}{V} - k - D - \zeta\right)\cdot n_i(t) + \frac{2\cdot\beta\cdot Q}{V}\cdot n_j(t) + \frac{2\cdot S + Q\cdot n_{sup}}{V} \quad (22)$$

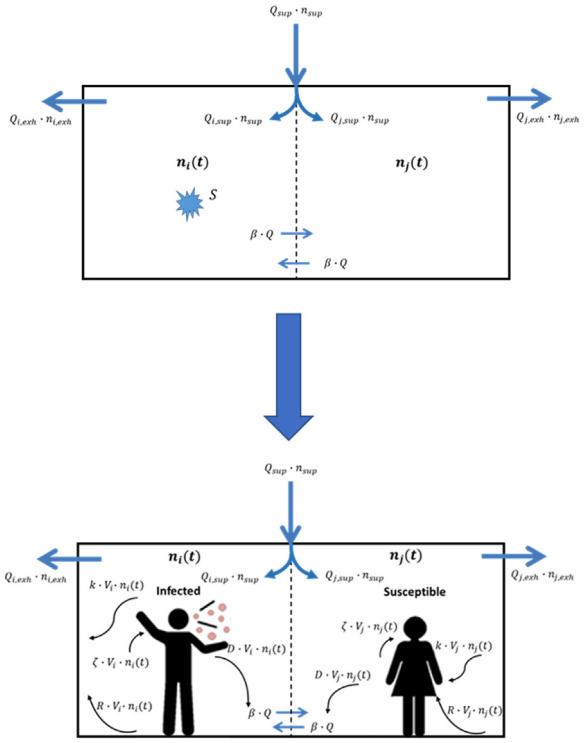

Fig. 8. Schematic representation of transforming the simplified two-zone model concept of contaminant distribution for protected [60] to a two-zone exposure model for assessing the long-range airborne transmission risks in indoor environments.

The quanta flow rate balance for the protected zone *j:*

$$V_j \cdot \frac{dn_j(t)}{dt} = Q_{j,sup} \cdot n_{sup}(t) + \beta \cdot Q \cdot n_i(t) - Q_{j,exh} \cdot n_{j,exh}(t) - \beta \cdot Q \cdot n_j(t) - k \cdot j(t) \cdot V_j - D \cdot V_j \cdot n_j(t) - \zeta \cdot V_j \cdot n_j(t) \tag{23}$$

=>

$$\frac{dn_j(t)}{dt} = \frac{2 \cdot Q \cdot \beta}{V} \cdot n_i(t) + \left(-\frac{2 \cdot Q \cdot \beta + Q}{V} - k - D - \zeta \right) \cdot n_j(t) + \frac{Q \cdot n_{sup}}{V} \tag{24}$$

For protected zone ventilation the mixing factor can be expressed as a function of the ventilation efficiency, as follows:

$$\beta = \frac{2}{4 \cdot \varepsilon - 3} \cdot \frac{Q + (k + D + \zeta) \cdot V}{Q} \tag{25}$$

$$\varepsilon = 0.11 \cdot \frac{Q}{V} + 0.21 \tag{26}$$

We used an experimental study by Aganovic & Cao [61] with n=9 data and the air change rates $\frac{Q}{V}$ to express the relationship between the ventilation efficiency. A linear regression model was fairly strong ($R^2 = 0.71$), Fig. 9.

2.7. Solutions for quanta concentrations for the two-zonal ventilation systems

The differential equations for the change in the quanta concentrations in zones *i* and *j*, i.e. the pair of Eqs. (8) and (10) for incomplete/imperfect mixing ventilation, Eqs. (16) and (18) for displacement ventilation, and Eqs. (22) and (24) for protected occupied zone ventilation can be written in the following forms:

$$\frac{dn_i(t)}{dt} = A_1 \cdot n_i(t) + B_1 \cdot n_j(t) + C_1 \tag{27}$$

$$\frac{dn_j(t)}{dt} = A_2 \cdot n_i(t) + B_2 \cdot n_j(t) + C_2 \tag{28}$$

Where the constant coefficients A_1,A_2,B_1,B_2, C_1 *and* C_2 for the ventilation systems are presented in Table 1:

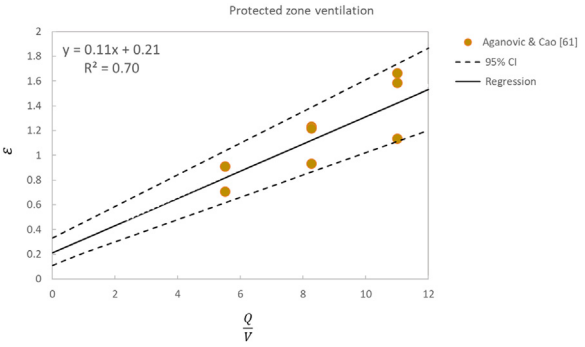

Fig. 9. A linear regression fit model for expressing the ventilation efficiency ε for protected zone ventilation.

Table 1
Constant coefficients for solving the coupled system of differential Eqs. (8) & (10), (16) & (18), (22) & (24).

Type of ventilation system	A_1	A_2	B_1	B_2	C_1	C_2
Incomplete mixing ventilation	$(-\frac{\beta\cdot Q\cdot H}{1.8\cdot V} - k - D - 2\cdot\zeta)$	$\frac{\beta\cdot Q\cdot H}{V\cdot(H-1.8)}$	$\frac{\beta\cdot Q\cdot H}{1.8\cdot V}$	$-\frac{(\beta+1)\cdot Q\cdot H}{V\cdot(H-1.8)} - k - D$	$\frac{S\cdot H}{1.8\cdot V}$	$\frac{Q\cdot n_{sup}\cdot H}{V\cdot(H-1.8)}$
Displacement ventilation	$-\frac{(\beta+1)\cdot Q\cdot H}{y_n\cdot V} - k - D - 2\cdot\zeta$	$\frac{(\beta+1)\cdot Q\cdot H}{V\cdot(H-y_n)}$	$\frac{\beta\cdot Q\cdot H}{y_n\cdot V}$	$(-\frac{(\beta+1)\cdot Q\cdot H}{V\cdot(H-y_n)} - k - D - 2\cdot\zeta)$	$\frac{(1-\Phi)\cdot S\cdot H}{y_n\cdot V} + \frac{Q\cdot n_{sup}\cdot H}{y_n\cdot V}$	$\frac{\Phi\cdot S\cdot H}{V\cdot(H-y_n)}$
Protected zone ventilation	$-\frac{2\cdot\beta\cdot Q+Q}{V} - k - D - \zeta$	$\frac{2\cdot Q\cdot\beta}{V}$	$\frac{2\cdot\beta\cdot Q}{V}$	$-\frac{2\cdot Q\cdot\beta+Q}{V} - k - D - \zeta$	$\frac{2\cdot S+Q\cdot n_{sup}}{V}$	$\frac{Q\cdot n_{sup}}{V}$

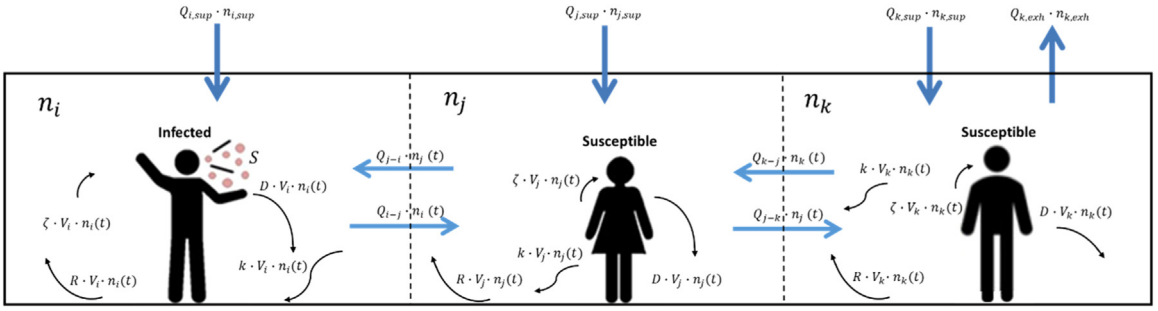

Fig. 10. Schematic representation of a simple indoor air mass-balance model in a three-zone model.

The unique solutions to this set of first-order differential Eqs. (27) and (28):

$$n_i(t) = K_1\cdot\left(\frac{r_1}{A_2}\cdot e^{r_1\cdot t} - \frac{B_2}{A_2}\cdot e^{r_1\cdot t}\right) + K_2\cdot\left(\frac{r_2}{A_2}\cdot e^{r_2\cdot t} - \frac{B_2}{A_2}\cdot e^{r_2\cdot t}\right) - \frac{B_2}{A_2}\cdot\frac{C_1\cdot A_2 - C_2\cdot A_1}{A_1\cdot B_2 - A_2\cdot B_1} - \frac{C_2}{A_2} \tag{29}$$

$$n_j(t) = K_1\cdot e^{r_1\cdot t} + K_2\cdot e^{r_2\cdot t} + \frac{C_1\cdot A_2 - C_2\cdot A_1}{A_1\cdot B_2 - A_2\cdot B_1} \tag{30}$$

Where $r_1 = \frac{A_1+B_2+\sqrt{(A_1+B_2)^2-4\cdot(A_1\cdot B_2-A_2\cdot B_1)}}{2}$ and $r_2 = \frac{A_1+B_2-\sqrt{(A_1+B_2)^2-4\cdot(A_1\cdot B_2-A_2\cdot B_1)}}{2}$

The coefficients K_2 and K_1 can be calculated using initial conditions $n_i(0) = 0$ and $n_j(0) = 0$:

$$K_2 = \frac{(C_1\cdot A_2 - C_2\cdot A_1)\cdot(r_1 - B_2) + C_1\cdot B_2 - C_2\cdot B_1}{(r_2 - r_1)\cdot(A_1\cdot B_2 - A_2\cdot B_1)} \tag{31}$$

$$K_1 = -K_2 - \frac{C_1\cdot A_2 - C_2\cdot A_1}{A_1\cdot B_2 - A_2\cdot B_1} \tag{32}$$

2.8. Three-zonal theoretical ventilation model

While the two-zone models described in previous chapters are characterized by one single supply airflow inlet, we here introduce a three-zone ventilation model capturing the airborne risk infection dynamics in an occupied room with three inlets and one outlet. The modeling approach presented in this chapter is based on a recent experimental study on the airborne transmission risk of SARS-Cov-2 using tracer gas measurements in an enclosed space with the same layout of airflow supply inlets and exhaust outlets [62]. The three-zone model based on the study is presented in Fig. 10.

Given that the supply airflow rates to each zone are equal $Q_{i,sup} = Q_{j,sup} = Q_{k,sup}$, and each zone has an equal volume $V_i = V_j = V_k = V$ the interzonal flow rate between zones i and j can be determined by $Q_{j-i} = Q_{i-j} + Q_{i,sup} = \beta \cdot Q + Q$ and the interzonal airflow rate between zones j an k can be determined by $Q_{j-k} + Q_{i,sup} = Q_{k-j} + Q_{k,exh} = > Q_{j-k} = \gamma \cdot Q + 2 \cdot Q$, where $Q_{k-j} = \gamma \cdot Q$. Both interzonal mixing factors β and γ were adjusted to fit the results based on the reported experimental measurements from the study [62].

The quanta flow rate balance for zone *i:*

$$V_i \cdot \frac{dn_i(t)}{dt} = S + Q_{i,sup} \cdot n_{i,sup}(t) + Q_{j-i} \cdot n_j(t) - Q_{i-j} \cdot n_i(t) - k \cdot n_i(t) \cdot V_i - D \cdot V_i \cdot n_i(t) - \zeta \cdot V_i \cdot n_i(t) \tag{33}$$

and after regrouping:

$$\frac{dn_i(t)}{dt} = \left(\frac{-\beta \cdot Q}{V} - k - D - \zeta \right) \cdot n_i(t) + \frac{(1+\beta) \cdot Q}{V} \cdot n_j(t) + \frac{S}{V} + Q \cdot n_{sup} \tag{34}$$

The quanta flow rate balance for zone *j:*

$$V_j \cdot \frac{dn_j(t)}{dt} = Q_{sup} \cdot n_{j,sup}(t) + Q_{i-j} \cdot n_i(t) + Q_{k-j} \cdot n_k(t) - Q_{j-i} \cdot n_j(t) - Q_{j-k} \cdot n_j(t) - k \cdot n_j(t) \cdot V_j - D \cdot V_j \cdot n_j(t) - \zeta \cdot V_j \cdot n_j(t) \tag{35}$$

$$\frac{dn_j(t)}{dt} = \frac{\beta \cdot Q}{V} \cdot n_i(t) + \frac{(-\beta - \gamma - 2) \cdot Q}{V} - k - D - \zeta \cdot n_j(t) + \left(\frac{\gamma \cdot Q}{V} \right) \cdot n_k(t) + Q \cdot n_{sup} \tag{36}$$

The quanta flow rate balance for zone *k:*

$$V_k \cdot \frac{dn_k(t)}{dt} = Q_{j-k} \cdot n_j(t) - Q_{k-j} \cdot n_k(t) - Q_{k,exh} \cdot n_k(t) + Q_{sup} \cdot n_{k,sup}(t) - k \cdot n_k(t) \cdot V_k - D \cdot V_k \cdot n_k(t) - \zeta \cdot V_k \cdot n_k(t) \tag{37}$$

$$\frac{dn_j(t)}{dt} = \frac{(\gamma + 2) \cdot Q}{V} \cdot n_j(t) + \frac{(-\gamma - 2) \cdot Q}{V} \cdot n_k(t) + Q \cdot n_{sup} \tag{38}$$

The differential equations for quanta concentrations in zones i, j, and k can be written in the following terms:

$$\frac{dn_i(t)}{dt} = A_1 \cdot n_i(t) + B_1 \cdot n_j(t) + C_1 \cdot n_j(t) + M \tag{39}$$

$$\frac{dn_j(t)}{dt} = A_2 \cdot n_i(t) + B_2 \cdot n_j(t) + C_2 \cdot n_k(t) + N \tag{40}$$

$$\frac{dn_k(t)}{dt} = A_3 \cdot n_i(t) + B_3 \cdot n_j(t) + C_3 \cdot n_k(t) + K \tag{41}$$

The equations can be written in the following form: $\boldsymbol{n}'(t) = \boldsymbol{A} \cdot \boldsymbol{n}(t) + \boldsymbol{b}(t)$ *where*

Let $\boldsymbol{n}(t) = \begin{matrix} n_i(t) \\ [n_j(t)] \\ n_k(t) \end{matrix}$ and $\boldsymbol{A} = \begin{matrix} A_1 & B_1 & C_1 \\ [A_2 & B_2 & C_2\,] \\ A_3 & B_3 & C_3 \end{matrix}$ and $\boldsymbol{b}(t) = \begin{matrix} M \\ [N] \\ K \end{matrix}$

The unique solution to this equation given initial conditions $n_i(t) = n_j(t) = n_k(t) = 0$ can be expressed as $\boldsymbol{n}(t) = \boldsymbol{n_c}(t) + \boldsymbol{n_p}(t)$

Where the fundamental matrix $\boldsymbol{\Phi}(t) = \begin{matrix} v_{11} \cdot e^{\lambda_1 t} & v_{12} \cdot e^{\lambda_2 t} & v_{13} \cdot e^{\lambda_3 t} \\ [v_{21} \cdot e^{\lambda_1 t} & v_{22} \cdot e^{\lambda_2 t} & v_{23} \cdot e^{\lambda_3 t}] \\ v_{31} \cdot e^{\lambda_1 t} & v_{32} \cdot e^{\lambda_2 t} & v_{33} \cdot e^{\lambda_3 t} \end{matrix}$ and λ_1,λ_2 *and* λ_3 are the three distinct real solutions of the characteristic polynomial of $\boldsymbol{A}$. where $\boldsymbol{v}_1 = \begin{matrix} v_{11} \\ [v_{21}] \\ v_{31} \end{matrix}$, $\boldsymbol{v}_2 = \begin{matrix} v_{21} \\ [v_{22}] \\ v_{32} \end{matrix}$ and $\boldsymbol{v}_3 = \begin{matrix} v_{31} \\ [v_{23}] \\ v_{33} \end{matrix}$ are associate eigenvectors (i.e. $A \cdot v_1 = \lambda_1 \cdot v_1$, $A \cdot v_2 = \lambda_2 \cdot v_2$ *and* $A \cdot v_3 = \lambda_3 \cdot v_3$).

Then the general solution is $\boldsymbol{n_c}(t) = K_1 \cdot \boldsymbol{v}_1 \cdot e^{\lambda_1 t} + K_2 \cdot \boldsymbol{v}_2 \cdot e^{\lambda_2 t} + K_3 \cdot \boldsymbol{v}_3 \cdot e^{\lambda_3 t}$ (42)

The particular solution is found as : $\boldsymbol{n_p}(\boldsymbol{t}) = \boldsymbol{\Phi}(t) \cdot \int \boldsymbol{\Phi}(t)^{-1} \cdot b(t) dt$ (43)

2.9. The source and removal terms in the extended Wells-Riley model

2.9.1. The source term S

The pollutant source emission rate S is defined as the quanta emission rate of SARS-CoV-2 generated by infected persons and can be defined by [18]:

$$S = I \cdot c_v \cdot c_i \cdot IR \cdot \sum_{i=1}^{n} (N_i \cdot V_i) \tag{44}$$

I – number of infected persons, -

c_v – viral load in the sputum, $\frac{RNA}{ml}$

The input data for c_v was based on recent data [63] for the mean viral of the delta variant, thus $c_v = 6.91 \cdot log_{10} \frac{RNA}{ml}$ was used as input in Eq. (4). But this value can also be determined for any other variant and virus type for which the viral load is known and the calculations are made.

c_i – conversion factor is defined as the ratio between one infectious quantum and the infectious dose expressed in viral RNA copies (quanta/RNA). Schijven et al. [64] developed a dose-response relationship for SARS-CoV-2 based on a SARS-CoV-2 isolate (hCoV-19/Netherlands/Zuid-Holland_10003/2020). It was estimated that $3.13 \cdot 10^9$ RNA replicates per mL match $5.62 \cdot 10^7$ tissue culture infectious doses that infect 50% of the cells ($TCID_{50}$) per ml. Based on these data the fraction of RNA viral copies that corresponds to 1 plaque-forming unit (PFU), given that $1\ PFU = 0.69\ TCID_{50}$ [65] conversion ratio is given by:

$$f = 0.69 \cdot \frac{5.62 \cdot 10^7}{3.13 \cdot 10^9} = 0.125$$

Given that Haas [66] recommended using the dose-response data for human coronavirus 229E (HCoV 229E) as representative for SARS-CoV-2 and that for each HCoV 229E eac hPFU has a probability of 0.055 to cause illness enables us to calculate that on average $\frac{1}{0.125 \cdot\ 0.055} = 1440$ viral copies per infectious dose of SARS-CoV-2. Therefore, we estimated $c_i = \frac{1\ quanta}{1440\ RNA} = 6.94 \cdot 10^{-4} \frac{quanta}{RNA}$.

IR – $(\frac{m^3}{h})$ – inhalation rate, i.e., the product of breathing (N_{br}) and tidal volume (V_{br}) –are both functions of the activity level of the infected subject. The inhalation rates for resting and standing averaged between males and females are equal to 0.49 and 0.54 $\frac{m^3}{h}$, respectively [67].

N_i- droplet number concentration in the ith bin, $\frac{particles}{cm^3}$

V_i – the mean volume of a single droplet (mL) in the ith bin.

$$V_i\ (D) = \frac{\pi \cdot \left(D_{max}^4 - D_{min}^4\right)}{24 \cdot (D_{max} - D_{min})} \tag{45}$$

where D_{max} and D_{min} denote the bin's lower and upper diameter values, according to Nicas [68].

i– size bin of the droplet distribution.

The size distribution of droplet aerosols $\leq 2\ \mu$m generated during talking is determined experimentally by the works of Morawska et al. [69] and for respiratory droplets $\geq\ 2\ \mu m$ by Chao et al. [70]. Both studies measured the size distribution of droplets for talking/voice counting at a distance of 10 mm from the participant's mouth opening. Therefore, the measured concentration of droplets represents the original size of the droplets at the mouth opening or the mass equivalent diameter of the particle D_{eq} (m) at the temperature and RH in the respiratory tract (37 °C and RH = 99.5%). The total volume of droplets was calculated by multiplying the droplet number distribution by the mean volume corresponding to each diameter in the size distribution [71].

2.9.2. Virus inactivation rate/biological decay constant k

To characterize the impact of relative humidity on the inactivation rate k, experimental data [72] on the survival time of SARS-CoV-2 in aerosols were aggregated for mean values of k (min^{-1}) at two indoor relative humidity values (RH=20% and RH=53%) $k_{RH\ =\ 20\%} = 0.0053\ min^{-1}$and at $k_{RH\ =\ 53\%} = 0.0101\ min^{-1}$.

2.9.3. The deposition rate D

The deposition rate D of a virus-laden droplet can be expressed as follows:

$$D = \frac{v_s}{H_{person}} \tag{46}$$

H_{person} – the average height of the infected person(s),m

The gravitational settling velocity of the droplets v_s and $\frac{m}{s}$ can be determined from the following:

$$v_s = \sqrt{\frac{4 \cdot \rho_d \cdot g \cdot D_{eq}}{3 \cdot \rho_a \cdot C_{d,s}}} \tag{47}$$

The relationship between the RH and equilibrium droplet diameter (D_{eq}) can be derived from the separate solute volume additivity (SS-VA) model for multi-component particles by Mikhailov et al. [73]. For the sake of brevity, the equations are not repeated here. All the equations can be found in a recent publication on the relationship between indoor RH and infection risk using the Wells-Riley model [71].

2.9.4. Respiratory tract absorption rate, ζ

Respiratory tract absorption rate, ζ ($\frac{1}{h}$) is a function of droplet diameter and tidal volume size [74] and can be calculated according to the following equation:

$$\zeta = \frac{DE \cdot IR}{V} \tag{48}$$

IR is the inhalation rate of the exposed subject (which was assumed to be the inhalation rate for resting and standing averaged) at 0.52 $\frac{m^3}{h}$, and *DE* (%) is the total deposition number that can be approximated by following analytical expression as a function of the equivalent droplet diameter:

$$DE(D_{eq}) = 1 - \frac{b}{\left(De_q \cdot 10^{-6} + d_0\right) \cdot \ln\left(s \cdot \sqrt{2 \cdot \pi}\right)} \cdot e^{\left[-\frac{1}{2} \cdot \left\{ \frac{\ln\left(De_q \cdot 10^{-6} + d_0\right) - \ln d_1}{\ln s} \right\}^2 \right]} \tag{49}$$

Where $b = 5.788$, $s = 2.574$, $d_0 = 1.2$ *and* $d_1 = 4.307$ are constant values for an average tidal volume of 500 ml which is considered in this study [75].

2.10. The infection risk calculation

To calculate the infection risk for the exposed person for complete, incomplete, and displacement ventilation we used $n(t) = n_i(t)$ while for protected occupied zone ventilation, we used $n(t) = n_j(t)$ in the Eq. (6). *IR* is the inhalation rate of the exposed person (which was assumed to be the inhalation rate for resting and standing averaged at 0.52 $\frac{m^3}{h}$, and *T* is the total exposure time (h).

The following scenarios are considered:

- 0.5, 2.0, 4.0, and 8.0 ACH for incomplete mixing ventilation at four different temperature differences between supply and exhaust air ($\Delta T = 0\ K$, $2\ K$, $5\ K$ *and* $10\ K$)
- 0.5 and 2.0 ACH for displacement ventilation (Section 3.2) at four different temperature differences between supply and exhaust air ($\Delta T = 0\ K$, $2\ K$, $5\ K$ *and* $10\ K$) and different standing and sitting positions for the infected and susceptible person
- 4.0 and 6.0 ACH protective zone ventilation
- 2.0 ACH for a large three-zone ventilation model.

The modeling approach is applied to a small room with one infected and one susceptible person present. The results are shown for a 40 m^2 x 3 m sized room with two occupants, one infected (RNA = $10^{6.91}\frac{RNA}{ml}$) and one susceptible person that is distanced by at least 1 m.

3. Results and discussion

3.1. Incomplete mixing ventilation

The results in Fig. 10 compare the incomplete mixing zonal models for three different temperature differences between the supply and exhaust air (ΔT=2 K,5 K, and 10 K) with the results of the complete mixing zonal model, i.e. the temperatures of the exhaust and supply air are equal (ΔT=0 K). Fig. 11 shows that the temperature difference has a notable impact on the infection risk when the air is heated compared to the isothermal air supply. Although the differences between infection risks are least noticeable for a high ventilation rate of 8.0 ACH, the relative difference can still have an important effect when comparing the results for ΔT=0 K and ΔT=10 K. Increasing supply temperature to ΔT=10 K higher than exhaust air relatively increases infection risk up to more than 15 % for low ventilation rates (0.5 ACH) and up to 10 % for higher ventilation rates (6 ACH) after 90 min compared to complete mixing (ΔT=10 K).

3.2. Displacement ventilation

For the case of displacement ventilation, the most important effect on the infection risk will be determined by the height of the neutral zone and the position of the breathing zone of both the infected and the susceptible person. Fig. 12 illustrates the infection risk when both persons are standing in a room with displacement ventilation. An increased ACH will significantly increase the neutral height position at higher supply airflow rates, resulting in lower infection risks. The impact of the temperature difference of supply and exhaust air on is more pronounced at lower ventilation rates (0.5 ACH).

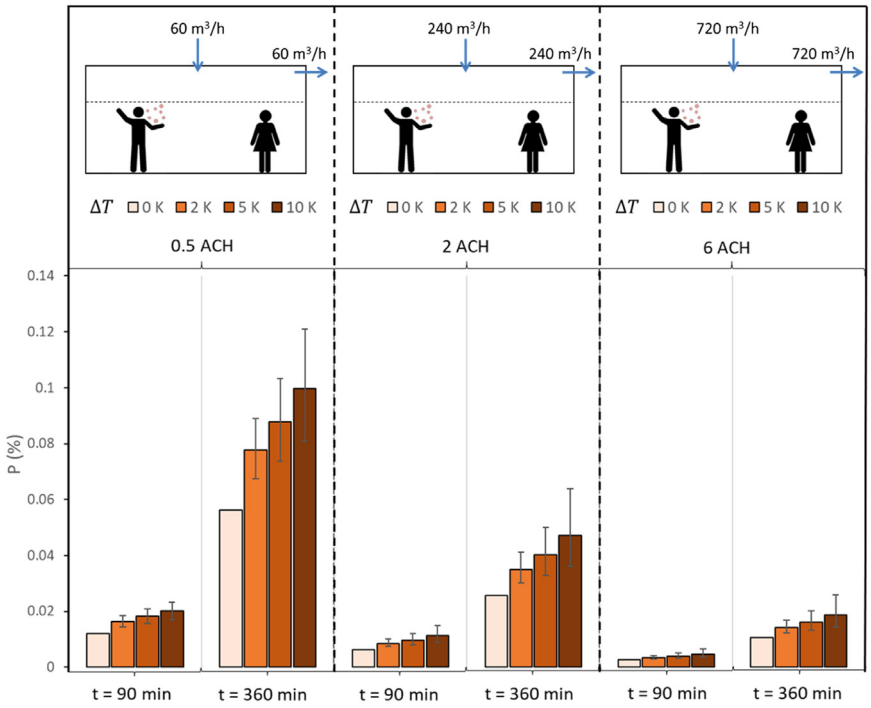

Fig. 11. infection risk $P(\%)$ for different scenarios of incomplete mixing ventilation systems. ΔT stand for the temperature difference between the supply and exhaust air. For $\Delta T = 0\,K\,(\beta \to \infty)$ complete mixing conditions occur. For $\Delta T \neq 0\,K$ error bars show 95 % confidence intervals as calculated for Eq. (11).

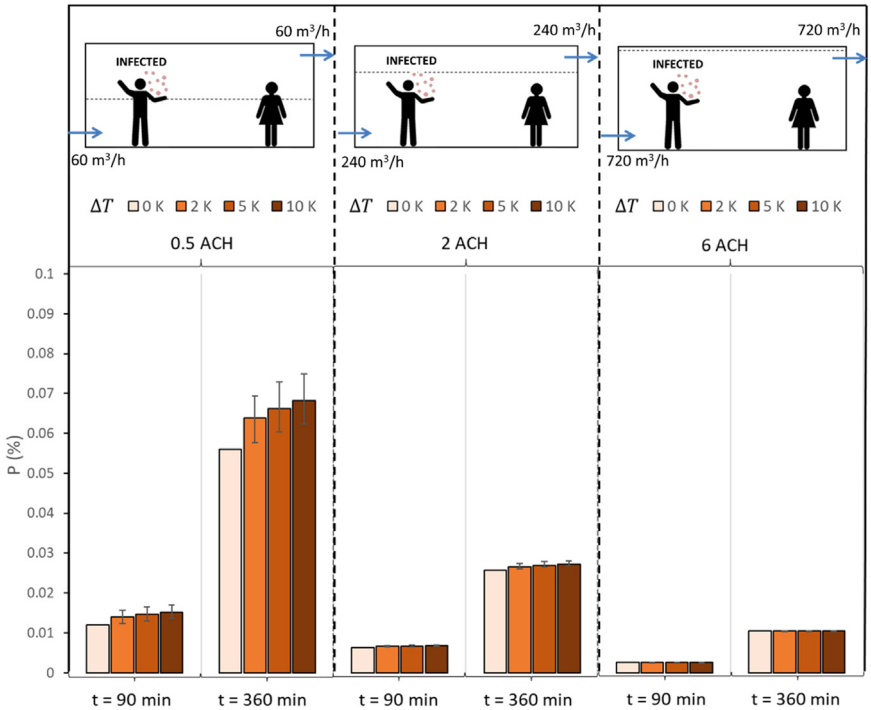

Fig. 12. infection risk $P(\%)$ for displacement ventilation when both the infected and susceptible person is standing. For $\Delta T = 0\,K\,(\beta \to \infty)$ complete mixing conditions occur. For $\Delta T \neq 0\,K$ error bars show 95 % confidence intervals as calculated for Eqn 20.

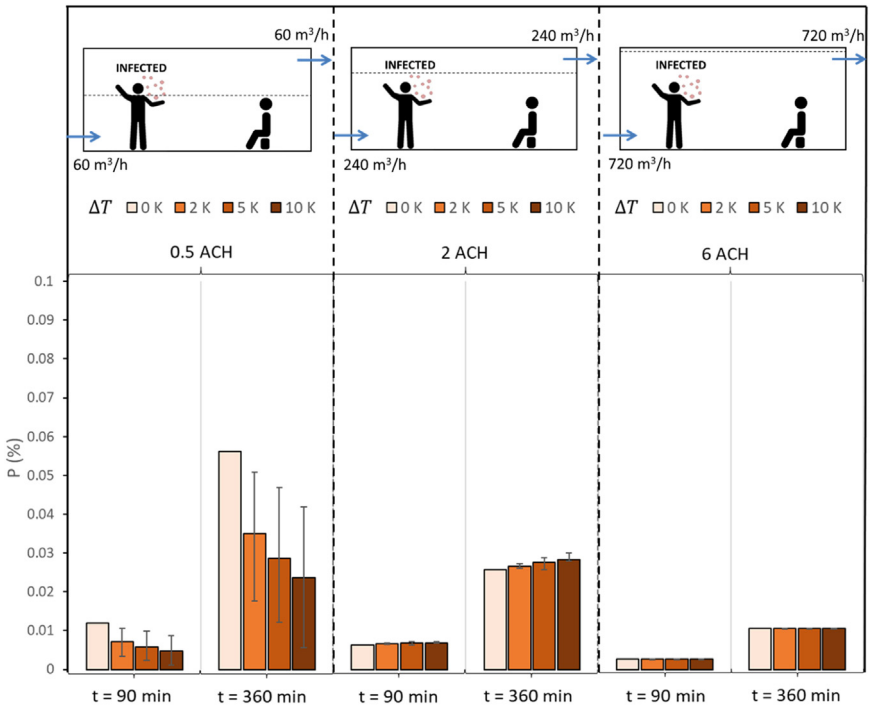

Fig. 13. infection risk $P(\%)$ for displacement ventilation when the infected person is standing and the susceptible person is sitting. For $\Delta T = 0\,K$ $(\beta \rightarrow \infty)$ complete mixing conditions occur. For $\Delta T \neq 0\,K$ error bars show 95 % confidence intervals as calculated for Eqn 20.

At 2.0 ACH, when the neutral zone is above the breathing zones of both persons, the impact of the temperature difference is very low, while at higher ventilation rates of 6 ACH the impact of ΔT on infection risk is almost insignificant.

The importance of considering the specific type of displacement ventilation instead of complete mixing ventilation is best illustrated in Fig. 13 when the breathing zone of the standing infected person is located in the upper contaminated zone while the breathing zone of the sitting susceptible person is located in the lower clean zone. In this case, the temperature difference has a very strong impact on the infection risk, reducing it by up to more than two times for high-temperature differences between supply and exhaust air (ΔT=10 K). However as the airflow rate increases, the height of the neutral zone increases. Most interestingly, when there is a temperature difference between the supply and exhaust air, the impact of increasing the ventilation rate by a factor of four (0.5 ACH $\rightarrow$ 2.0 ACH) will not considerably lower the infection risk. In fact, at a higher temperature difference (ΔT=10 K) the infection risk might be lower at lower ventilation rates (0.5 ACH) compared to the calculated infection risks at 2.0 ACH. Also, as in the previous case, when both the breathing zones of the infected and susceptible person are in the same zone that happens for higher ventilation rates, the impact of the temperature difference between the supply and exhaust air is almost negligible.

3.3. *Protected zone ventilation with exhaust located in the ceiling*

The case of protected zone ventilation in Fig. 14 shows that the infection risk in the protected zone with the susceptible person will be reduced compared to complete mixing conditions and that the tendency of reducing the infection spread is increasing with increased ventilation rate (0.5 ACH $\rightarrow$ 2.0 ACH $\rightarrow$ 6 ACH).

The accuracy levels were expressed in form of 95 % confidence intervals as calculated for the derived mixing factors for the two-zone models' Eq. (11) for incomplete mixing ventilation, Eq. (19) for displacement ventilation model, and Eq. (25) for protective zone ventilation. For all two-zone ventilation systems, the results showed that the range values of the calculated 95 % CI for the modeled infection risk were either entirely above the infection risk for complete mixing ventilation (as shown in Fig. 11 for incomplete mixing ventilation, Fig. 12 for displacement ventilation when the susceptible person is standing and Fig. 14 for the polluted zone for protected zone ventilation) or the 95 % CI range values were entirely below the complete mixing infection risk (as shown in Fig. 13 for displacement ventilation when the susceptible person is sitting and Fig. 14 for the protected zone for protected zone ventilation). This implies that the wide range of 95 % CI values was still predicting the infection risk consistently for the predicted regression Eqs. (11), (19), and (25) shown by the colored data bars in each of Figs. 11–14.

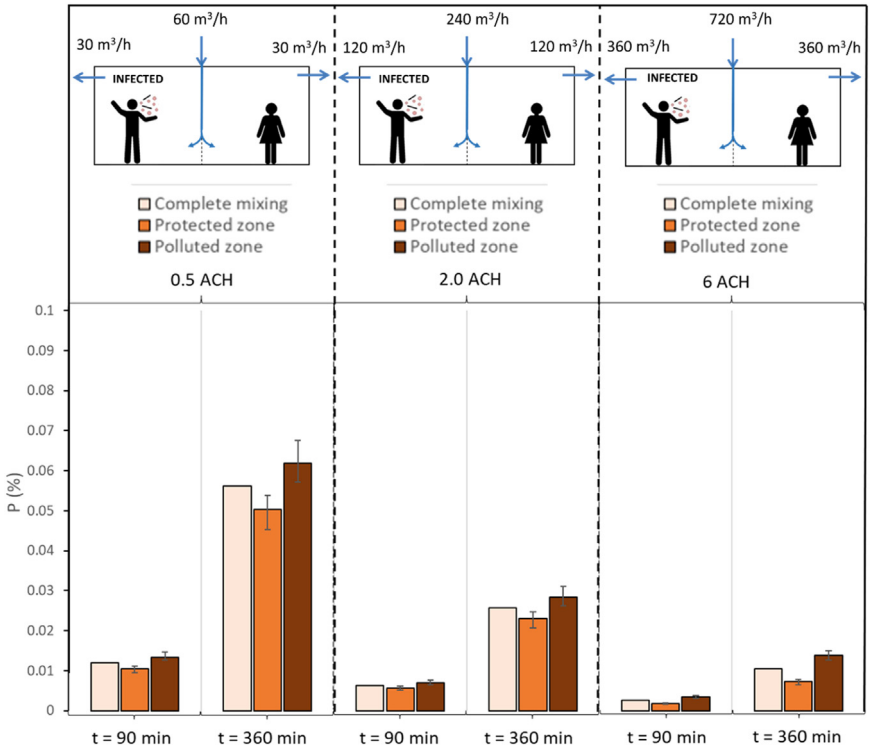

Fig. 14. infection risk P (%) for protected zone ventilation. conditions occur. Error bars show 95 % confidence intervals as calculated for Eqn 26.

Table 2
Relative comparison of the infection risk overestimation (+)/underestimation (-) of a two-zone airflow distribution method compared to completely mixed single-zone airflow distribution.

Incomplete mixing ventilation			
	$\Delta T = 2\ K$	$\Delta T = 5\ K$	$\Delta T = 10\ K$
0.5 ACH	+ 38.4 %	+ 56.3 %	+ 77.5 %
2.0 ACH	+ 36.2 %	+ 56.0 %	+ 82.8 %
6.0 ACH	+ 34.1 %	+ 52.9 %	+ 78.7 %
Displacement ventilation (infected person standing / susceptible person standing)			
	$\Delta T = 2\ K$	$\Delta T = 5\ K$	$\Delta T = 10\ K$
0.5 ACH	+ 13.8 %	+ 18.0 %	+ 21.5 %
2.0 ACH	+ 3.5 %	+ 4.8 %	+ 5.9 %
6.0 ACH	+ <0.1 %	+ < 0.1 %	+ < 0.1 %
Displacement ventilation (infected person standing / susceptible person sitting)			
	$\Delta T = 2\ K$	$\Delta T = 5\ K$	$\Delta T = 10\ K$
0.5 ACH	- 37.7 %	- 49.0 %	- 59.7 %
2.0 ACH	+ 3.5 %	+ 4.7	+ 5.9 %
6.0 ACH	+ <0.1 %	+ < 0.1 %	+ < 0.1 %
Protected zone ventilation (protected zone)			
0.5 ACH	-10.4 %		
2.0 ACH	-10.5 %		
6.0 ACH	- 30.9 %		

3.4. Relative comparison of two-zone model calculated infection risk compared to the conventional completely mixed single-zone Wells-Riley model

Table 2 shows the airflow distribution method compared to completely mixed single-zone airflow distribution. The relative difference (%) of the infection risks calculated is expressed as

$$\frac{P_{two-zone} - P_{completely\ mixing\ single\ zone}}{P_{completely\ mixing\ single\ zone}}$$

after 360 min of exposure for the considered scenario. ΔT is the temperature difference between the supply and exhaust/room temperatures.

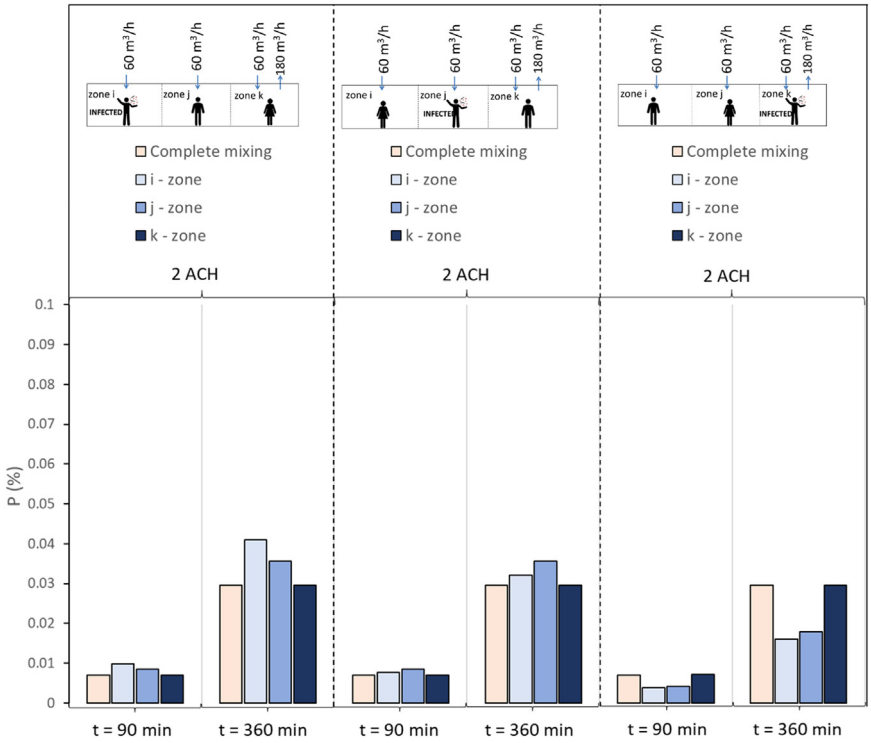

Fig. 15. infection risk P(%) for a zonal ventilation system when the infected person is located in each of the three zones

The single-zone Wells-Riley model based on a completely mixing assumption relatively overestimates the infection risk by at least 34 % for the case when the supply air is heated (i.e. incomplete mixing ventilation) regardless of the ventilation rate. The overestimation may also be higher by at least 13 % compared to displacement ventilation when the susceptible person is standing and at low ventilation rates (0.5 ACH). With higher ventilation rates the relative overestimation drops below 6 % at 2.0 ACH and becomes almost negligible at 6.0 ACH (<0.1 %). The underestimation of the infection risk is high for low ventilation rate (0.5 ACH) displacement ventilation when the person is standing, ranging between 37.7 and 59.7 % depending on the supply of air and temperature difference. Once again as in the case of when the susceptible person is sitting, the relative overestimation is below 6 % at 2.0 ACH and becomes almost negligible at 6.0 ACH (<0.1 %). For protected zone ventilation the Wells-Riley model based on completely mixing conditions may underestimate the infection risk for at least 10 % at 0.5 and 2.0 ACH, and up to more than 30 % at higher ventilation rates (6.0 ACH).

3.5. Three zonal ventilation model

The three zonal ventilation models are shown in Fig. 15. It depicts the infection risk for three different positions of the infected person in each of the three zones. It is shown that the infection risk in the zone with both supply and exhaust (zone k) is equal for all three scenarios, regardless of the infected person's position and it is equal to the infection risk that would exist for complete mixing conditions. However, the infection risk in the other two zones with only supply inlets (i and j) are strongly influenced by the position of the infected person. Only when the infected person is in the zone with both supply and exhaust, will this type of ventilation system reduce the infection risk in the other two zones compared to complete mixing conditions. For the other two cases shown on the left and middle part of Fig. 14, the infection risk will be higher in the or best case scenario equal to the infection risk for complete mixing ventilation conditions. Thus, when calculating the infection risk in larger spaces with a non-uniform distribution of the supply and exhaust outlets in the ceiling, using the Wells-Riley model based on the assumption of complete mixing may considerably over-or underestimate the infection risk.

4. Model limitations

There are several limitations of our model:

1 Our model applies only to the long-distance airborne transmission of SARS-CoV-2. Short-range is not dealt with.
2 The impact of convective flows within the space caused by thermal sources such as human thermal plumes on the flow field has been ignored. As a result, our method may not be suitable for highly occupied spaces and needs to be extended for such situations.

3 It is assumed that occupants remain where they are most of the time i.e. the occupant activities are not considered. Moving occupants can increase mixing between zones on the one hand and also increase the infection risk generating directional transportation of exhaled virus-laden aerosols.
4 We have transformed a three-dimensional problem into a two-dimensional problem.
5 The linear regression relationships developed for correlating the ventilation efficiency and indoor environment parameters (12), (20), and (26) may be subject to inaccuracy as they are compiled from studies with different experimental setups.
6 The zones have been firmly defined and mixing within a single zone may not be achieved completely. Other room sizes have not been taken into account.
7 The assumption that expelled aerosol droplets are evenly distributed in the air of the room implies that there is an immediate dilution of the expelled virus concentration. In reality, dilution will not occur instantaneously; it highly depends on the movement of the air in the room. Even in a well-mixed room, an exposed person standing directly in front of the infected person may inhale a much larger dose of airborne particles than an exposed person physically distanced at least 1 m apart.
8 The resuspension effect has been excluded as a removal mechanism in our version of the Wells-Riley model as previous studies on the airborne transmission of respiratory diseases have shown that disease transmissions could depend on the resuspension of floor dust [76].
9 The values calculated with this model could vary significantly as a function of the activity levels of both the infected subject and the viral load in the sputum of the infected subject.
10 The infected individual was assumed to talk constantly, which may present an unrealistic overproduction of the number of respiratory droplets expelled.
11 The probability of infection calculated according to Eq. (6) is strongly dependent on the dose-response relationship c_i. To allow for a more absolute comparison between infection risks from different studies, other assessment methods, which are independent of the dose-response data [74,77] should also be considered in future studies.
12 The validation of any Wells-Riley model for calculating airborne infection risk would require detailed input parameters from an actual outbreak and this is complex for several reasons. This method requires considerable input information from the observed outbreaks, including the type of ventilation system, ventilation rates, space volume, and exposure time of infected persons but also additional building system details such as the amount of recirculated air, filter efficiency, etc.. As there is no source providing this information the airborne risk calculation cannot be sure. Future outbreak reports must include this information for validated retrospective infection risk assessments.

5. Conclusions

The findings of the zonal analytical modeling of the infection risk in rooms occupied by an infected and susceptible person and the exposure time up to 6 h can be summarized in the following key points.

- Incomplete mixing
  - The results of our model showed that increasing the temperature difference between supply and exhaust air ΔT increases the infection risk for incomplete mixing conditions compared to completely mixing conditions (ΔT=0 K).
  - The single-zone Wells-Riley model may relatively underestimate the infection risk by a substantial amount compared to the two-zone incomplete mixing model.
- Displacement ventilation
  - The relative difference to complete mixing conditions is mostly caused by the position of the neutral plane that depends on the heat load, amount of supplied air, and temperature difference between supply and exhaust air.
  - The single-zone Wells Riley model may considerably underestimate the infection risk when the susceptible person is standing at low ventilation rates (0.5 ACH). On contrary, when the susceptible person is sitting the conventional complete mixing model may overestimate the infection risk to a great extent. Regardless of whether the susceptible person is sitting or standing, the relative underestimation is low at 2.0 ACH and becomes almost negligible at 6.0 ACH (<0.1 %).
- Protective zone ventilation
  - Protective zone ventilation decreases the infection risk in the protected zone with the susceptible person while it increases the infection risk in the polluted zone compared to completely mixing conditions.
  - For protected zone ventilation the Wells-Riley model based on completely mixing conditions may overestimate the infection risk to considerable extents at all ventilation rates of 0.5 to 6.0 ACH.
- Three-zone model
  - A case study with a three-zone model shows the importance of the zonal distribution of ceiling supply inlets and exhaust outlets compared to completely mixing conditions. In this case, it is also important to consider the relative position of the infected person.

In conclusion, this study shows that using the Wells-Riley model based on the assumption of completely mixing air may overestimate the long-range airborne infection risk compared to some high-efficiency ventilation air distribution systems such as displacement ventilation and protected zone ventilation, but also underestimate the infection risk

in a room heated with warm air supplied from the ceiling. Therefore, when assessing long-range airborne transmission risk of infectious respiratory diseases a zonal modeling approach should be preferred in analytical models compared to the conventional single-zone Wells-Riley models in indoor spaces where the room air and supply air is not completely mixed.

Data availability

Data will be made available on request.

References

[1] https://covid19.who.int/
[2] https://www.cdc.gov/coronavirus/2019-ncov/science/science-briefs/sars-cov-2-transmission.html
[3] L. Morawska, D.K. Milton, It is time to address airborne transmission of coronavirus disease 2019 (COVID-19), Clin. Infect. Dis. 71 (2020) 2311–2313 pmid:32628269CrossRefPubMedGoogle Scholar, doi:10.1093/cid/ciaa939.
[4] L. Morawska, J. Cao, Airborne transmission of SARS-CoV-2: the world should face the reality, Environ. Int. 139 (2020) 105730 pmid:32294574CrossRefPubMedGoogle Scholar, doi:10.1016/j.envint.2020.105730.
[5] J.A. Lednicky, M. Lauzard, Z.H. Fan et al. Viable SARS-CoV-2 in the air of a hospital room with COVID-19 patients.
[6] R. Zhang, Y. Li, A.L. Zhang, Y. Wang, M.J. Molina, Identifying airborne transmission as the dominant route for the spread of COVID-19, Proc. Natl. Acad. Sci. 117 (26) (2020) 202009637.
[7] J.W. Tang, W.P. Bahnfleth, P.M. Bluyssen, et al., Dismantling myths on the airborne transmission of severe acute respiratory syndrome coronavirus-2 (SARS-CoV-2), J. Hosp. Infect. 110 (2021) 89–96, doi:10.1016/j.jhin.2020.12.022.
[8] T. Greenhalgh, J.L. Jimenez, K.A. Prather, Z. Tufekci, D. Fisman, R. Schooley, Ten scientific reasons in support of airborne transmission of SARS-CoV-2, Lancet 397 (10285) (2021) 1603–1605 May 1Epub 2021 Apr 15. Erratum in: Lancet. 2021 May 15;397(10287):1808. PMID: 33865497; PMCID: PMC8049599, doi:10.1016/S0140-6736(21)00869-2.
[9] V.C.C. Cheng, et al., Nosocomial outbreak of COVID-19 by possible airborne transmission leading to a superspreading event, Clin. Infect. Dis. (2021) ciab313 an official publication of the Infectious Diseases Society of America14 Apr., doi:10.1093/cid/ciab313.
[10] L. Morawska, J. Allen, W. Bahnfleth, et al., A paradigm shift to combat indoor respiratory infection, Science 372 (6543) (2021) 689–691 May 14PMID: 33986171, doi:10.1126/science.abg2025.
[11] W.F. Wells, Airborne Contagion and Air Hygiene: An Ecological Study of Droplet Infections, Harvard University Press, 1955.
[12] E.C. Riley, G. Murphy, R.L. Riley, Airborne spread of measles in a suburban elementary school, Am. J. Epidemiol. 107 (1978) 421–432.
[13] B. Patterson, C.D. Morrow, D. Kohls, C. Deignan, S. Ginsburg, R. Wood, Mapping sites of high TB transmission risk: Integrating the shared air and social behaviour of TB cases and adolescents in a South African township, Sci. Total Environ. 583 (2017) 97–103 Apr 1Epub 2017 Jan 18. PMID: 28109661; PMCID: PMC5312671, doi:10.1016/j.scitotenv.2017.01.026.
[14] P. Azimi, Z. Keshavarz, J.G. Cedeno Laurent, J.G. Allen, Estimating the nationwide transmission risk of measles in US schools and impacts of vaccination and supplemental infection control strategies, BMC Infect. Dis. 20 (1) (2020) 497, doi:10.1186/s12879-020-05200-6.
[16] X. Gao, J. Wei, B.J. Cowling, Y. Li, Potential impact of a ventilation intervention for influenza in the context of a dense indoor contact network in Hong Kong, Sci. Total Environ. 569-570 (2016) 373–381 Nov 1Epub 2016 Jun 25. PMID: 27351145, doi:10.1016/j.scitotenv.2016.06.179.
[16] B.G. Wagner, B.J. Coburn, S. Blower, Calculating the potential for within-flight transmission of influenza A (H1N1), BMC Med. 7 (2009) 81 Dec 24PMID: 20034378; PMCID: PMC2813231, doi:10.1186/1741-7015-7-81.
[17] A. Aganovic, Y. Bi, G. Cao, J. Kurnitski, P. Wargocki, Modeling the impact of indoor relative humidity on the infection risk of five respiratory airborne viruses, Sci Rep. 12 (2022) 11481, doi:10.1038/s41598-022-15703-8.
[18] G. Buonanno, L. Morawska, L. Stabile, Quantitative assessment of the risk of airborne transmission of SARS-CoV-2 infection, Environ. Int. 145 (2020) 106112.
[19] A.A. Aliabadi, S.N. Rogak, K.H. Bartlett, S.I. Green, Preventing airborne disease transmission: review of methods for ventilation design in health care facilities, Adv. Prev. Med. 2011 (2011) 124064, doi:10.4061/2011/124064.
[20] G.N. Sze To, C.Y. Chao, Review and comparison between the Wells-Riley and dose-response approaches to risk assessment of infectious respiratory diseases, Indoor Air 20 (1) (2010) 2–16 FebEpub 2009 Jul 31. PMID: 19874402; PMCID: PMC7202094, doi:10.1111/j.1600-0668.2009.00621.x.
[21] L. Gammaitoni, M.C. Nucci, Using a mathematical model to evaluate the efficacy of TB control measures, Emerg. Infect. Dis 3 (1997) 335–342, doi:10.3201/eid0303.970310.
[22] S.N. Rudnick, D.K. Milton, Risk of indoor airborne infection transmission estimated from carbon dioxide concentration, Indoor Air 13 (3) (2003) 237–245 SepPMID: 12950586, doi:10.1034/j.1600-0668.2003.00189.x.
[23] A.K. Melikov, Advanced air distribution: improving health and comfort while reducing energy use, Indoor Air 26 (1) (2016) 112–124 FebEpub 2015 Apr 23. PMID: 25833265, doi:10.1111/ina.12206.
[24] G. Cao, H. Awbi, R. Yao, Y. Fan, K. Sirén, R. Kosonen, J.J. Zhang, A review of the performance of different ventilation and airflow distribution systems in buildings, Build. Environ. 73 (2014) 171–186.
[25] A.K. Melikov, Z.T. Ai, D.G. Markov, Intermittent occupancy combined with ventilation: An efficient strategy for the reduction of airborne transmission indoors, Sci. Total Environ. 744 (2020) 140908, doi:10.1016/j.scitotenv.2020.140908.
[26] G. Ko, K.M. Thompson, E.A. Nardell, Estimation of tuberculosis risk on a commercial airliner, Risk Anal. 24 (2) (2004) 379–388, doi:10.1111/j.0272-4332.2004.00439.x.
[27] C.J. Noakes, P.A. Sleigh, Applying the Wells-Riley equation to the risk of airborne infection in hospital environments: the importance of stochastic and proximity effects, in: Proceedings of the 11th International Conference on Indoor Air Quality and Cl. Indoor Air 2008, Copenhagen, Denmark., Copenhagen, 2008 17-22nd August.
[28] C.J. Noakes, P.A. Sleigh, Mathematical models for assessing the role of airflow on the risk of airborne infection in hospital wards, J. R. Soc. Interface 6 (2009) S791–S800.
[29] C.J. Noakes, A. Khan, C.A. Gilkeson, et al., Modeling infection risk and energy use of upper-room ultraviolet germicidal irradiation systems in multi-room environments, Sci Technol Built Environ. 21 (1) (2015) 99–111, doi:10.1080/10789669.2014.983035.
[30] C.J. Noakes, C.B. Beggs, P.A. Sleigh, Modelling the performance of upper room ultraviolet germicidal irradiation devices in ventilated rooms, Comp. Anal. CFD Methods Indoor Built Environ. 13 (6) (2004) 477–488.
[31] Y. Guo, et al., Assessing and controlling infection risk with Wells-Riley model and spatial flow impact factor (SFIF), Sustain. Cities Soc. 67 (2021) 102719.
[32] Y. Yan, X. Li, Y. Shang, J. Tu, Evaluation of airborne disease infection risks in an airliner cabin using the Lagrangian-based Wells-Riley approach, Build. Environ. 121 (2017) 79–92, doi:10.1016/j.buildenv.2017.05.013.
[33] H. Qian, Y. Li, P.V. Nielsen, X. Huang, Spatial distribution of infection risk of SARS transmission in a hospital ward, Build. Environ. 44 (8) (2009) 1651–1658, doi:10.1016/j.buildenv.2008.11.002.2.

[34] J.K. Gupta, C.H. Lin, Q. Chen, Risk assessment of airborne infectious diseases in aircraft cabins, Indoor Air 22 (5) (2012) 388–395, doi:10.1111/j.1600-0668.2012.00773.x.
[35] Y. Zhang, X. Li, X. Wang, W. Deng, K. Qian, Spatial flow influence factor: a novel concept for indoor air pollutant control, Sci. China Ser. E 49 (1) (2006) 115–128, doi:10.1007/s11431-004-5247-x.
[36] X. Wang, W. Tao, Y. Lu, F. Wang, A method to identify the point source of indoor gaseous contaminant based on limited on-site steady concentration measurements, Build. Simul. 6 (4) (2013) 395–402, doi:10.1007/s12273-013-0127-6.
[37] X. Li, D. Lester, G. Rosengarten, C. Aboltins, M. Patel, I. Cole, A spatiotemporally resolved infection risk model for airborne transmission of COVID-19 variants in indoor spaces, Sci. Total Environ. 812 (2021) 152592 Dec 23Epub ahead of print. PMID: 34954184; PMCID: PMC8695516, doi:10.1016/j.scitotenv.2021.152592.
[38] S. Zhang, Z. Lin, Dilution-based evaluation of airborne infection risk - thorough expansion of Wells-Riley model, Build. Environ. 194 (2021) 107674, doi:10.1016/j.buildenv.2021.107674.
[39] M. Nicas, Estimating exposure intensity in an imperfectly mixed room, AIHAJ 57 (1996) 542–550.
[40] M. Sandberg, What is ventilation efficiency, Build. Environ. 16 (1981) 123–135, doi:10.1016/0360-1323(81)90028-7.
[41] K.K. Coleman, D.J.W. Tay, K.S. Tan, et al., Viral load of severe acute respiratory syndrome Coronavirus 2 (SARS-CoV-2) in respiratory aerosols emitted by patients With Coronavirus Disease 2019 (COVID-19) while breathing, talking, and singing, Clin. Infect. Dis. (2021) ciab691, doi:10.1093/cid/ciab691.
[42] Z. Ai, K. Hashimoto, A.K. Melikov, Airborne transmission between room occupants during short-term events: measurement and evaluation, Indoor Air 29 (4) (2019) 563–576.
[43] R.R. Netz, Mechanisms of airborne infection via evaporating and sedimenting droplets produced by speaking, J. Phys. Chem. B 124 (33) (2020) 7093–7101 Aug 20Epub 2020 Jul 31. PMID: 32668904; PMCID: PMC7409921, doi:10.1021/acs.jpcb.0c05229.
[44] Z. Ai, C.M. Mak, N. Gao, J. Niu, Tracer gas is a suitable surrogate of exhaled droplet nuclei for studying airborne transmission in the built environment, Build. Simul. (2020) 1–8, doi:10.1007/s12273-020-0614-5.
[45] M. Bivolarova, J. Ondráček, A. Melikov, V. Ždímal, A comparison between tracer gas and aerosol distribution indoors: the impact of ventilation rate, interaction of airflows, and presence of objects, Indoor Air J. 27 (6) (2017) 1201–1212.
[46] M. Krajcik, A. Simone, B.W. Olesen, Air distribution and ventilation effectiveness in an occupied room heated by warm air, Energy Build. 55 (2012) 94–101.
[47] B.W. Olesen, A. Simone, M. Krajčík, F. Causone, M. De Carli, Experimental study of air distribution and ventilation effectiveness in a room with a combination of different mechanical ventilation and heating/cooling systems, Int. J. Vent. 9 (2011) 371–383.
[48] R. Cermak, A.K. Melikov, Air quality and thermal comfort in an office with underfloor, mixing, and displacement ventilation, Int. J. Vent. 5 (3) (2006) 323–332.
[49] P.V. Nielsen, Displacement Ventilation, Dept. of Building Technology and Structural Engineering, 1993 Indoor Environmental Engineering No. 15.
[50] W. Ye, Y. Pan, L. He, B. Chen, J. Liu, J. Gao, Yi Wang, Y. Yang, Chapter 3 - Design with modeling techniques, in: H.D. Goodfellow, Y. Wang (Eds.), Industrial Ventilation Design Guidebook, 2nd Ed., Academic Press, 2021, pp. 109–183.
[51] T.H. Dokka (2000). Modelling of indoor air quality in residential and commercial buildings. (Doctoral dissertation). Retrieved from https://brage.bibsys.no/xmlui/handle/11250/265599
[52] J.J. Sacco, J. Botten, F. Macbeth, A. Bagust, P. Clark, The average body surface area of adult cancer patients in the UK: a multicentre retrospective study, PLoS One 5 (1) (2010) e8933 Jan 28PMID: 20126669; PMCID: PMC2812484, doi:10.1371/journal.pone.0008933.
[53] H. Brohus, P.V. Nielsen, Personal exposure in displacement ventilated rooms, Indoor Air 6 (1996) 157–167.
[54] M. Xu, T. Yamanaka, H. Kotani, Vertical profiles of temperature and contaminant concentration in rooms ventilated by displacement with heat loss through room envelopes, Indoor Air 11 (2001) 111–119.
[55] R.B. Holmberg, L. Eliasson, K. Folkesson, Strindehag, Inhalation zone air quality provided by displacement ventilation, in: Proceedings of the International Conference on Air Distribution in Ventilated Spaces, Room Vent '90, Oslo, Norway, 1990.
[56] B. Halvonova, A.K. Melikov, Performance of ductless personalized ventilation in conjunction with displacement ventilation: impact of workstations layout and partitions, HVAC & R Res. 16 (1) (2010) 75–94.
[57] R. Cermak, A.K. Melikov, L. Forejt, O. Kovar, Performance of personalized ventilation in conjunction with mixing and displacement ventilation, Int. J. Heat. Vent. Refrig. Res. 12 (2) (2006) 295–311.
[58] M. Xu, T. Yamanaka, H. Kotani, T. Higashimoto, Effect of cooled or heated wall on vertical distribution of temperature and contaminant concentration in rooms with displacement ventilation, J. Archit. Plan. Environ. Eng. 544 (2001) 17–23.
[59] E. Bjørn, P.V. Nielsen, Dispersal of exhaled air and personal exposure in displacement ventilated rooms, Indoor Air 12 (3) (2002) 147–164.
[60] G. Cao, K. Sirén, S. Kilpeläinen, Modelling and experimental study of performance of the protected occupied zone ventilation, Energy Build. 68 (2014) 515–531, doi:10.1016/j.enbuild.2013.10.008.
[61] A. Aganovic, G. Cao, Evaluation of airborne contaminant exposure in a single-bed isolation ward equipped with a protected occupied zone ventilation system, Indoor Built Environ. 28 (8) (2019) 1092–1103, doi:10.1177/1420326X18823048.
[62] R. Simson, M. Kiil, K.V. Võsa, A. Kesküll, J. Kurnitski, Assessment of SARS-CoV-2 transmission in room with mixing ventilation using CO_2 tracer gas technique, in: Proceedings of the Healthy Buildings America, Honolulu, Hawaii, USA, International Society of Indoor Air Quality and Climate (ISIAQ), 2022 2021January 18-20, 2022.
[63] C. von Wintersdorff, J. Dingemans, L. van Alphen et al. Infections caused by the Delta variant (B.1.617.2) of SARS-CoV-2 are associated with increased viral loads compared to infections with the Alpha variant (B.1.1.7) or non-Variants of Concern., 04 August 2021, PREPRINT (Version 1) available at Research Square 10.21203/rs.3.rs-777577/v1
[64] J. Schijven, L.C. Vermeulen, A. Swart, A. Meijer, E. Duizer, A.M. de Roda Husman, Quantitative microbial risk assessment for airborne transmission of SARS-CoV-2 via breathing, speaking, singing, coughing, and sneezing, Environ. Health Perspect. 129 (4) (2021) 47002, doi:10.1289/EHP7886.
[65] M.A. Ramakrishnan, Determination of 50% endpoint titer using a simple formula, World J. Virol. 5 (2) (2016) 85–86 May 12PMID: 27175354; PMCID: PMC4861875, doi:10.5501/wjv.v5.i2.85.
[66] C.N. Haas, Action levels for SARS-CoV-2 in air: preliminary approach, Risk Anal. 41 (5) (2021) 705–709 MayEpub 2021 Apr 5. PMID: 33818802; PMCID: PMC8251121, doi:10.1111/risa.13728.
[67] W.C. Adams, 1993. Measurement of breathing rate and volume in routinely performed daily activities. Final Report. Human Performance Laboratory, Physical Education Department, University of California, Davis. Human Performance Laboratory, Physical Education Department, University of California, Davis. Prepared for the California Air Resources Board, Contract No. A033-205, April 1993.
[68] M. Nicas, W.W. Nazaroff, A. Hubbard, Toward understanding the risk of secondary airborne infection: emission of respirable pathogens, J. Occup. Environ. Hyg. 2 (3) (2005) 143–154 MarPMID: 15764538; PMCID: PMC7196697, doi:10.1080/15459620590918466.
[69] L. Morawska, G.R. Johnson, Z.D. Ristovski, M. Hargreaves, K. Mengersen, S. Corbett, C.Y.H. Chao, Y. Li, D. Katoshevski, Size distribution and sites of origin of droplets expelled from the human respiratory tract during expiratory activities, J. Aerosol Sci., 40 (2009) 256–269, doi:10.1016/j.jaerosci.2008.11.002.
[70] Chao et al., 2009 C.Y.H. Chao, M.P. Wan, L. Morawska, G.R. Johnson, Z.D. Ristovski, M. Hargreaves, K. Mengersen, S. Corbett, Y. Li, X. Xie, D. Katoshevski, Characterization of expiration air jets and droplet size distributions immediately at the mouth opening, J. Aerosol Sci. 40 (2009) 122–133.
[71] A. Aganovic, Y. Bi, G. Cao, F. Drangsholt, J. Kurnitski, P. Wargocki, Estimating the impact of indoor relative humidity on SARS-CoV-2 airborne transmission risk using a new modification of the Wells-Riley model, Build. Environ. 205 (2021), doi:10.1016/j.buildenv.2021.108278.
[72] C.B. Beggs, E.J. Avital, A psychrometric model to assess the biological decay of the SARS-CoV-2 virus in aerosols, PeerJ 9 (2021) e11024 Published 2021 Mar 2, doi:10.7717/peerj.11024.
[73] E. Mikhailov, S. Vlasenko, R. Niessner, U. Poschl, Interaction of aerosol particles composed of protein and salts with water vapor: Hygroscopic growth and microstructural rearrangement, Atmos. Chem. Phys. 4 (2004) 323–350.

[74] B. Jones, P. Sharpe, C. Iddon, E.A. Hathway, C.J. Noakes, S. Fitzgerald, Modelling uncertainty in the relative risk of exposure to the SARS-CoV-2 virus by airborne aerosol transmission in well mixed indoor air, Build. Environ. 191 (2021) 107617, doi:10.1016/j.buildenv.2021.107617.
[75] J. Heyder, G. Rudolf, Deposition of aerosol particles in the human nose, Inhaled Part. 4 (Pt 1) (1975) 107–126 SepPMID: 1236151.
[76] P. Khare, L.C. Marr, Simulation of vertical concentration gradient of influenza viruses in dust resuspended by walking, Indoor Air 25 (4) (2015) 428–440 AugEpub 2014 Oct 3. PMID: 25208212, doi:10.1111/ina.12156.
[77] Y. Li, H. Qian, J. Hang, X. Chen, P. Cheng, H. Ling, S. Wang, P. Liang, J. Li, S. Xiao, J. Wei, L. Liu, B. Cowling, M. Kang, Probable airborne transmission of SARS-CoV-2 in a poorly ventilated restaurant, Build. Environ. 196 (2021) 107788, doi:10.1016/j.buildenv.2021.107788.